Report
P-21-02
May 2021

Fracture toughness using pseudo-compact tension (*p*CT) test and semi-circular bending specimen (SCB) test

Jordi Delgado-Martín
Andrea Muñoz-Ibáñez
Miguel Herbón-Penabad
Leandro R Alejano

SVENSK KÄRNBRÄNSLEHANTERING AB

SWEDISH NUCLEAR FUEL
AND WASTE MANAGEMENT CO

Box 3091, SE-169 03 Solna
Phone +46 8 459 84 00
skb.se

SVENSK KÄRNBRÄNSLEHANTERING

ISSN 1651-4416
SKB P-21-02
ID 1923520

May 2021
Updated 2021-09

Fracture toughness using pseudo-compact tension (*p*CT) test and semi-circular bending specimen (SCB) test

Jordi Delgado-Martín, Andrea Muñoz-Ibáñez,
Miguel Herbón-Penabad

Civil Engineering School, University of A Coruña

Leandro R Alejano, Department of Natural Resources and Environmental Engineering, University of Vigo

Keywords: Mode I fracture toughness, *p*CT test, SCB test, Acoustic emission.

Update notice

The original report, dated May 2021, was found to contain both factual and editorial errors which have been corrected in this updated version. The corrected factual errors are presented below.

Updated 2021-09

Location	Original text	Corrected text
Cover and title page	Two authors missing	Two authors added

Abstract

Twelve fracture toughness (K_C) tests of specimens in granite to granodiorite (rock type 101057), sampled from a ground surface rock block of the Forsmark future high-level radioactive waste disposal site, have been performed using the ISRM's SCB suggested method and the results have been compared with the newly developed *p*CT test methodology. Details about test execution are presented as well as a procedure for the assessment of the validity of test results. According with this procedure, with the exception of one *p*CT sample, all the tests performed were acceptable. However, two more SCB specimens were discarded based on textural and mineralogical representativeness considerations. The statistical assessment of the data shows that the fracture toughness results obtained with the two testing methodologies are comparable and the mean value for the 101057 rock is 1.59 ± 0.09 MPa $m^{1/2}$. Furthermore, AE data concurrent with mechanical testing provide deeper insights in the case of *p*CT than in the case of the SCB method.

Sammanfattning

Tolv provningar av brottseghet (K_C) har utförts på prover i granit till granodiorit (bergartskod 101057), tagna från ett bergblock på markytan i Forsmark vid platsen för det framtida slutförvaret för använt kärnbränsle. Provningen är utförd enligt ISRM:s föreslagna metod, SCB, och resultatet har jämförts med resultat från den nyligen utvecklade *p*CT-provningsmetoden. Detaljer avseende provningarnas genomförande och proceduren för att utvärdera provningsresultatet redovisas. I enlighet med denna procedur gav alla provningar, med undantag för ett *p*CT-prov, godkända resultat. Två ytterligare SCB-prov uteslöts dock från sammanställningen på grund av att mineralogi och textur i proven bedömdes mindre representativa. Den statistiska utvärderingen av data visar att brottsegheten som bestämts med de två skilda metoderna är jämförbara och att medelvärdet för bergart 101057 är 1.59 ± 0.09 MPa $m^{1/2}$. Därtill visas att AE-data (Acoustic Emission) insamlad samtidigt med brottseghetsprovningen ger djupare förståelse i fallet med *p*CT jämfört med då SCB-metoden tillämpats.

Contents

1 Introduction

Fracture toughness (K_C) represents the ability of a material to resist crack initiation and propagation. Although it is a strength-related property, testing requires specially conditioned samples in which cracks are geometrically constrained to develop in a prescribed direction (i.e., with a starter notch) in order to apply the fundamental approaches of fracture mechanics (Ouchterlony 1988). Several testing methods with well-defined sample geometries are currently in use in rock mechanics to determine mode I fracture toughness (K_{IC}) in rocks. The International Society for Rock Mechanics (ISRM) endorses four of them considering cores as the preform for all the tested samples: Short Rod (SR), Chevron Bend (CB), Cracked Chevron Notched Brazilian Disc (CCNBD) and the Semi-Circular Bend (SCB) methods (Ouchterlony 1988, 1989, Fowell 1995, Kuruppu et al. 2014). Recently Muñoz-Ibáñez et al. (2020) have introduced the pseudo-compact tension (*p*CT) test as an alternative to overcome some of the drawbacks associated with the mentioned suggested methods (e.g., large sample size and cumbersome preparation). The claimed advantages of *p*CT would include: a) reduced rock requirement (disc-shaped specimen with a diameter-to-thickness ratio of 2); b) simple sample preparation (straight groove and thin starter notch); c) enhanced control of crack propagation (especially beyond peak strength); and d) pure tensile loading.

In this report we present the results of the experimental measurement of mode-I fracture toughness of selected samples of an igneous rock relevant to the future underground radioactive waste repository of Forsmark. The study is based on a limited number of tests considering the ISRM-suggested SCB method (Kuruppu et al. 2014) as well as recent *p*CT alternative (Muñoz-Ibáñez et al. 2020).

The information obtained provides with site-specific reference data useful to elaborate (or to constrain) more accurate geomechanical models and predictions. Both aspects contribute to a better understanding of the behaviour of granitic rocks in Forsmark within the context of the ongoing engineering and safety studies for the disposal of spent nuclear fuel conducted by SKB.

2 Materials and methods

2.1 Rock blocks

Eight equal-size parallelepipeds or slab-like rock pieces (40 × 30 × 22.5 cm) were received at the facilities of the Rock Mechanics Laboratory (LaMeRoc) on March 18th, 2019 (Figure 2-1). Each block was labelled according with the corresponding rock domain ID (RFM029 and RFM045) and block number (A, B, C and D). The blocks were sawed from large size rock boulders sampled within the rock domains RFM029 and RFM045. According to SKB (2013), each rock domain encompasses a group of lithologies presenting significant variations in mineralogy, grain size, texture and fabric (rock units). These blocks were previously used to drill cores of different lengths and diameters within the context of an investigation concerning scale effects on unconfined compressive (UCS) and Brazilian indirect tension strength (BTS) tests (Delgado and Alejano 2021)

For the present investigation and, in agreement with SKB, it was decided to conduct the fracture toughness tests with some of the remaining cores of rock type RFM029 which have not been used previously.

Based on SKB expert judgement, the likely rock type associated with RFM029 is 101057. The texture and fabric of this material is characterised by a penetrative ductile deformation under amphibolite-facies metamorphism. From a petrological point of view, it is a fine- to medium-grained metagranodiorite (to granite) with a moderately to strongly developed planar (to some extent linear) mineral fabric. It is characterised by a texture of stretched, monomineralic domains and a content of ferromagnesian minerals ranging up to 10 vol.% (SKB 2013). Table 2-1 summarises different physical and mechanical properties of the rock used in the present investigation, based on laboratory testing on samples from the same blocks.

At first glance, all the rock blocks received looked like solid and massive although a closer inspection revealed the existence of randomly oriented interlocked cracks cross cutting some of the blocks.

Table 2-1. Representative properties of rock RFM029.

Property	Value	Property	Value
ρ_{dry} (kg/m^3)	2 639.9 ± 1.8	V_P (m/s)	5 126 ± 19
H_2O (%)	0.12 (*0.00–0.44*)	V_S (m/s)	3 166 ± 19
ϕ (%)	0.32 (*0.00–1.16*)	V_P/V_S	1.62 (*1.57–1.72*)
UCS (MPa)	166.0 ± 4.6	E	86.7 ± 4.7
T (MPa)	14.2 ± 2.1	ν (–)	0.31 ± 0.02

Notes: ρ_{dry} = dry density; H_2O = water absorption; ϕ = porosity; V_P = compressive wave velocity; V_S = shear wave velocity; UCS = unconfined compressive strength; T = tensile strength; E = static Young's modulus; ν = static Poisson's ratio.

Figure 2-1. *Rock blocks as received: RFM029 on the left and RFM045 on the right.*

2.2 Core drilling, cutting and trimming

Coring was performed with the aid of a *WEKA DK32* diamond drill motor (*WEKA Elektrowerkzeuge e.K.*) attached to a DM 350BC mast located above the rock blocks. The obtained cores were cut to lengths compatible with the requirements established in the reference procedures for fracture toughness testing (see later). Plugs were cut with a 350 mm diamond saw disk (*Carat* mod. P-3500) and then trimmed with a manual drill (*Optimum BF-16V*) equipped with a lapping diamond disk to ensure the required flatness and parallelism between faces.

Based on the recommendations to conduct the fracture toughness tests, the selected cores to obtain the specimens were 63 and 100 mm-diameter. However, because the present survey was designed after completion of the UCS and BTS survey, only a limited number of specimens could be recovered. Table 2-2 summarises them.

Table 2-2. Specimens of rock RFM029 used to conduct SCB and *p*CT tests.

Specimen	Test	Diameter (mm)	Rock block
63-1, 63-2, 63-3, 63-6	*p*CT	63	C
63-11, 63-12	*p*CT	63	B
100-1A, 100-1B, 100-3A, 100-3B	SCB	100	C
100-8A, 100-8B	SCB	100	B

2.3 Core plug handling

Since there were no specific prescription of SKB concerning fracture toughness testing, the specimens were handled according to ISRM recommendations and procedures for the SCB tests, and based on the experience acquired during the development of the *p*CT test method. Furthermore, guidelines for data reporting were kept consistent with those described by SKB for other testing methods (e.g., SKB MD 190.001e ver. 4.0 and SKB 190.004e ver. 3.0, for UCS and BTS testing, respectively). Thus, the selected cores were: a) cut to lengths consistent with testing recommendations (length/diameter, L/D = 0.5 of both SCB and *p*CT), b) dry and wet-weighted; and c) submersed in tap water at room temperature during more than 7 days.

2.3.1 Geometrical properties of the samples

Plug dimensions were determined with the aid of a Vernier calliper (*Mitutoyo mod. 500-197-20*; resolution = 0.01 mm) and a precision digital height gage (*Shahe mod. 5324-150A*; resolution = 0.01 mm). Before the determinations, the measuring equipment was checked using a reference standard plug of 25.4 mm length and 12.7 mm diameter. All the measurements were conducted in a 400 × 400 mm flatness table (*Unceta Lan-Flat*®; flatness error = 2.9 mm).

2.3.2 Density, water absorption and porosity

The weight of the tested samples was determined with the aid of an internally calibrated digital precision scale (*Sartorius Entris 4502*; precision = 0.01 g) which was further verified with a reference standard weight. The weight of the samples was measured dry (after drying in an oven at 110 °C for more than 24 h) and moist (after immersion in water during more than 7 days).

2.4 Testing equipment

According to Ouchterlony (1988), fracture toughness investigations in rocks can be conducted with the suggested methods according to two testing levels:

- Level I (or screening level) provides fast and relatively simple access to material properties. In this level, only the maximum load (P_{max}) needs to be measured.
- Level II (or advanced level) takes into account the non-linear behavior that many rocks present. That level allows for a more detailed insight about the mechanics of the fracturing processes by continuously monitoring both the load and displacement beyond P_{max}.

Although the equipment described next can perform both levels of testing, in this investigation we report results based on Level I testing. Reasons for that are described in following sections.

2.4.1 Semi-cylinder bending (SCB) testing

SCB tests were performed with the aid of a multipurpose frame developed by *LaMeRoc* (Figure 2-2). This is a closed-loop servo electric device designed to conduct tests under load, displacement or strain control under static or dynamic conditions. The reaction platens of the frame were manufactured in AA7075-T6 aluminum alloy ($E = 71.7$ GPa, $\nu = 0.33$, $\sigma_{yield} = 503$ MPa) and they are connected with four 12.9 steel quality, M32 threaded bars (DIN 975). These are pre-stressed against four squared S275 structural steel tubes.

The frame is equipped with a primary (built in) 100 kN load cell (*AEP Transducers mod. CTC4127100KNI15*) which is calibrated to its mid-range (50 kN) to gain resolution. It may incorporate a secondary unit of lower capacity (from a few N to several kN) that can be attached or detached at convenience what allows a wide loading range without sacrificing accuracy. For the SCB tests reported in this investigation, no secondary load cell was used.

Figure 2-2. *General view of the test frame used to conduct the SCB tests (left) and detail of the testing fixture (right).*

For displacement/strain control the frame counts with a dual system based on: a) an encoder internal to the servo motor; and b) a magnetorestrictive linear position sensor (*MTS Temposonics* mod. EP 2003). Both systems operate in a maximum range of 200 mm.

The synchronous servo motor (*Lenze* MCS 06I41) is fed with AC (175V, 2.9A) and has nominal power and torque of 0.64 kW and 1.50 Nm. It is joined to a precision planetary gearhead (*Lenze* g700-P130; i =120) which extends the torque of the motor to 120 Nm. The servomotor and gearhead drive a 500 mm length ballscrew (*Hiwin* R32-05) with 32 mm diameter and 5 mm lead that is housed in a multipurpose tool post. The pair motor/ballscrew is attached to a stiff bracket that moves smoothly along two 25 mm linear guides (*Hiwin* HGH-CA).

The bottom platen is made of a general purpose carbon steel (F114/C45) threaded to the primary load cell. It incorporates centring pins for fixtures such the one illustrated in Figure 2-1.

The electronics of the frame is based on the PCD 2K software (*Servosis S.L.*) and allows to work under the control of the main or secondary load cell systems, integrating the signal of up to 16 analogue acquisition or mathematical channels. This system can operate either on force, displacement or strain controls, with programmable monotonic/cyclic procedures and control switching (i.e. from load to strain control). It is able to acquire with high-frequency the signals provided by a variety of sensors (force, displacement, temperature, pressure, strain gages, etc.).

For the present study, the control mode was set to displacement and monitoring included the record of the applied load and displacement of the actuator. Complementary, acoustic emissions (AE) were also recorded in each one of the SCB tests performed (see the description of the AE equipment in Section 2.4.3). In order to synchronise time in the load and acoustic emission systems, an analogue signal output corresponding to the measured load was directed to the AE system.

The data files obtained after each test were later filtered and post-processed in order to obtain the required properties. Post processing was performed with the aid of different *Microsoft™ Excel®* worksheets and then plotted with the software *Grapher®* 12.7 by *Golden Software Inc*.

Performance checking

All the measurement devices used in the present study were checked in order to evaluate their adequate performance and sensitivity. Checks were conducted at the instrument and electronic levels. With respect to the first approach, the load frame and control devices were calibrated by an external accredited service. The results of the calibration are presented in Appendix 1 and, as a summary, the SCB testing frame conforms to Class 1 force according with the standard UNE-EN-7500-1-2018 (UNE 2018) and Class A displacement for the two displacement devices (encoder and linear transducer) with respect the standard ASTM E2309-18 (ASTM 2018).

Characteristics of the specimens

The geometrical properties of the specimens used for SCB testing are indicated in Figure 2-3. The ISRM recommendations indicate that samples to be used in SCB fracture toughness tests should have a diameter of no less than 76 mm (or 10 times the largest crystal size) and a thickness no less than 0.4 times the corresponding diameter, with a minimum of 30 mm. Furthermore, the starter notch should be cut with a blade of no more than 1.5 ± 0.2 mm thickness and its depth constrained by the ratio between notch length (a) and sample radius (R) to a value between 0.4 and 0.6.

To conduct the SCB tests with rock 101057, the diameter and thickness of the selected plugs were of ~100 and ~48 mm, with a ratio a/R of ~0.55. The thickness of the diamond blade used to cut the starter notch was 1 mm. All these values are satisfactory with respect the previously given recommendations.

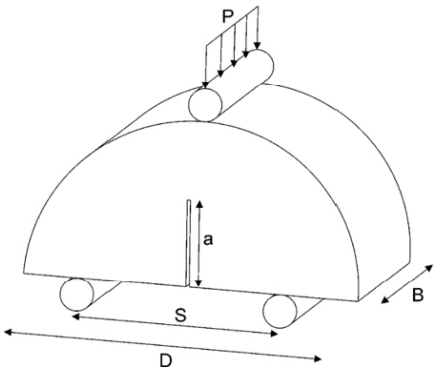

Figure 2-3. *Schematic illustration of the geometry of the SCB specimen. Notes: P = applied vertical load; D = specimen diameter; B = specimen thickness; a = starter notch length; S = span length.*

Testing procedures

SCB tests were carried out according to the indications given in Kuruppu et al. (2014) and summarised in Table 2-3. All the recorded parameters were acquired at a sampling frequency of 50 Hz.

The ISRM recommendation indicates that the span length (i.e., distance separating the supporting rolls) should be commensurate with the specimen diameter so that the corresponding S/D ratio should be comprised between 0.5 and 0.8, depending on the strength of the tested material. Likewise, the testing displacement speed should be less than 0.2 mm/min. As a summary of the tests performed, the S/D ratio used to conduct the tests with the RFM029 specimens was of ~0.8 (consistent with high strength rocks) while the displacement rate was set to 0.1 mm/min. Both parameters agree with the ISRM recommendations.

Table 2-3. SCB testing procedure.

Step	Description
1	Digital photos are taken of the specimen before the mechanical testing. The sample is equipped with a 6 mm-diameter magnet (which is glued with cyanoacrylate) that is used to attach the acoustic emission sensor.
2	The tested specimen is located over the hardened rollers of the three-point bending fixture and its notch centered with respect the vertical loading axis.
3	The loading roll of the testing fixture is lowered to a short distance (~0.5 mm) above the top of the specimen.
4	The stress (load) and LPD (linear displacement sensor) measurement channels are zeroed in the data acquisition software.
5	The beginning of the test is concurrent to recording. Recorded data includes load, load point displacement (LPD), AE activity, etc. The test is executed in displacement-control mode at a constant rate of 0.1 mm/min (0.0017 mm/s).
6	The test is stopped manually (switch off) after peak load has been observed and the specimen fails and falls apart.
7	Digital photos of the broken specimen are taken and the remnants recovered for provisional storage.
8	The system is disassembled and carefully cleaned for the next test.

Data processing

According to Kuruppu et al. (2014), the computation of mode I fracture toughness (K_{IC}) for the SCB test can be performed based on the following equation:

$$K_{IC}^{SCB} = Y'_{SCB} \frac{P_{max}\sqrt{\pi a}}{2RB}$$

where P_{max} is the peak load (in N), a is the notch length (in m), R and B are the specimen radius and thickness (both in m), respectively, and Y'_{SCB} is the specific non-dimensional stress intensity factor associated with the SCB method. This is given by the following expression:

$$Y'_{SCB} = -1.297 + 9.516\left(\frac{S}{2R}\right) - \left(0.47 + 16.457\left(\frac{S}{2R}\right)\right)\beta + \left(1.071 + 34.401\left(\frac{S}{2R}\right)\right)\beta^2$$

in which S is the span length (in m) and β the notch length ratio (β = a/R*)*. The corresponding units of K_{IC} are MPa $m^{1/2}$.

2.4.2 Pseudo-compact tension (*p*CT) testing

The pseudo-compact tension (*p*CT) test is based on an adaptation of the compact tension (CT) specimen described in the ASTM E399-12 (ASTM 2012) standard method for testing metallic materials and the testing principle is outlined in Figure 2-4. The two loading holes of the CT specimen are replaced by a groove. In addition, a thin radial notch is cut to act as stress concentrator and to provide the location for crack initiation.

Once the specimen is ready for testing, carrying out the test follows a simple and straightforward procedure. The specimen is mounted on a centring cradle and put in contact with a pair of high-strength, high-stiffness steel jaws that fit into the groove and transmit the tensile load to the sample. While one of the jaws remains in a static position, the other one is pulled away at a constant displacement rate. The tensile load within the thin notch tends to split the specimen into two symmetrical halves. The crack initiates at the notch tip and propagates along the vertical diameter of the specimen (i.e., the ligament plane). With this basic configuration, the bottom of the sample is not affected by other loads that its own self-weight.

The testing device consists of a high-stiffness frame (AA7075-T6; E = 71.7 GPa, ν = 0.33, σ_{yield} = 503 MPa) equipped with a 50 kN push/pull load cell (*AEP Transducers mod. CTC412750KNI15)*, two linear variable differential transducers (*Solartron LVDT G-series* AX/5/S), and two clip-on (COD) gages (*Epsilon Technology Co.*mod. 3541 and *MTS Co.* mod. 632.02). Electric signals from all the measurement devices are integrated into a dedicated data acquisition system (*GW Instruments Inc.* instruNet 3.6). The two LVDTs, placed symmetrically on both sides on the specimen, measure the load point displacement (LPD). Simultaneously, a clip-on gage mounted on a pair of bolt-on knife edges attached to the steel jaws measures the same magnitude for redundancy. An additional COD gage can be mounted directly on the surface of the specimen to measure the crack mouth opening displacement (CMOD). In the *p*CT configuration CMOD can be readily compared with LPD.

The movement of the steel jaw is accomplished by means of a 5-mm lead spindle (NBS mod. VFU 40005 DIN 69051 Form B), which converts the rotatory motion of an electric stepper motor (*Teco Electro Devices Co.* mod. DST56EL61A) with a step angle of 1.8° (i.e., 200 steps per revolution) into linear displacement. To improve its performance, the motor is connected to a planetary gearhead (*McLennan Servo Supp.* mod. IP-57-M2-100) with a reduction ratio of 1:100. This configuration provides a high degree of accuracy in positioning (0.018°/step), equivalent to 0.25 μm/step in terms of linear movement of the shaft, which can be maintained from 0 to 50 kN.

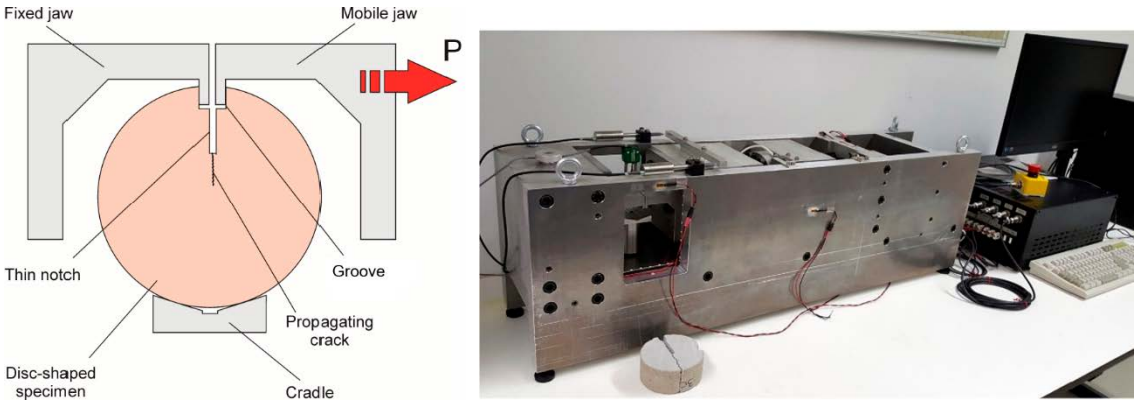

Figure 2-4. *Conceptual scheme of the pCT test (left) and frame used to conduct the experiments.*

The control system consists of: (i) an Arduino-based microcontroller (which commands the motor with a specific program, and keeps track of the displacements and safety signals delivered by the endstops) and (ii) dedicated software (that makes it possible to set up a testing path). Control commands are transmitted in real time to the microcontroller, which executes them and returns state and displacement data.

A stainless steel bellow coupling with a clamping hub (*StS Couplings* mod. WK4/60-89-SX 49/15,) connects the motor and the spindle. A fixed-side round-type support bearing (*Hiwin* FK30-C5) provides both axial and rotational support for the spindle.

The data files obtained after each test were later filtered and post-processed in order to obtain the required properties. Post processing was performed with the aid of different *Microsoft™ Excel®* worksheets and plotting with the software *Grapher®* 12.7 by *Golden Software Inc.*

Characteristics of the specimens

The *p*CT specimen is a cylindrical, disc-shaped sample that can be cut from rock cores. Its geometrical properties of the specimens used for *p*CT testing are indicated in Figure 2-5. This is based on the work of Muñoz-Ibáñez et al. (2020). According with them, the *p*CT samples used should have a recommended diameter of 50 mm and a thickness to diameter ratio of 0.5.

Finally, the ratio between the starter notch length and the distance from the base of the groove to the bottom of the specimen (a/b) should be greater than 0.25.

For the specimens of rock RFM029 the diameter and thickness of the samples were ~64 and ~30 mm respectively, with a ratio a/b of ~0.25. Like in the SCB tests, the thickness of the diamond blade used to cut the starter notch was 1 mm.

Performance checking

The experimental device is a non-standard system whose independent sensors can be independently calibrated. However, as a whole, the performance of the testing system is much more difficult to assess. The aspect with more direct impact over the results is system stiffness and that was investigated at the time of design and after construction using a double experimental/modeling approach.

The stiffness of the loading frame was investigated to assess its elastic energy storage during operation. To this aim, a neoprene layer was compressed between the two steel jaws to a load far above the usual working loads (~ 25 kN). The frame was instrumented with a total of eight 350 Ω strain gauges glued with cyanoacrylate onto the frame at critical points of its geometry. For the load applied, the maximum stress recorded at any point of the frame was 10.36 MPa, well below the endurance limit stress (100–150 MPa) provided by the fatigue design curves of AA7075-T6.

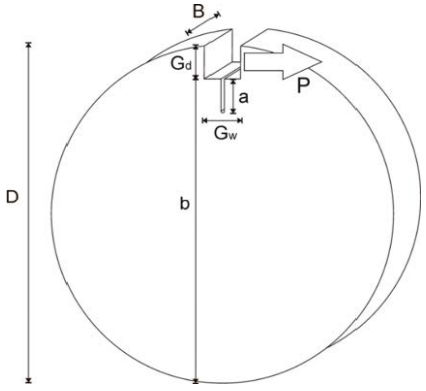

Figure 2-5. *Schematic illustration of the geometry of the pCT specimen. Notes: P = applied horizontal load; D = specimen diameter; B = specimen thickness; a = starter notch length; G_d = groove depth; G_w = groove width; b = distance from the base of the groove to the bottom of the specimen.*

To further investigate the performance of the device, a 3D finite element model was created in *Abaqus*/Standard version 6.14 (ABAQUS 2014) to simulate the previous test. The system was modelled as ten separate parts, including the frame, the two steel jaws, and the spindle. The bolted connections in the device were modelled by applying rigid body constraints in the holes, assuming that no relative displacement arises between the parts at the connecting points. The two materials in the machine (F1270 steel and AA7075-T6 aluminum), were modelled with a hypoelastic–perfectly plastic constitutive model, assuming elastic moduli of 210 and 71.7 GPa, and Poisson's ratios of 0.3 and 0.33, respectively.

The von Mises yield surface was adopted in both cases with associated plastic flow, and the initial yield stresses were 503 MPa for AA7075-T6 aluminum and 700 MPa for F1270 steel. Notice that this rather simple plasticity model was adopted only to verify that no plastic deformation took place in the machine during normal operation; therefore, a detailed description of the work hardening and the plastic flow was not necessary. The frame and the jaws were meshed with 10-node quadratic tetrahedrons, while the spindle was modelled with hexahedral elements with eight nodes and reduced integration, with the customary hourglass control.

The obtained displacement and stress distributions are presented in Figure 2-6. Due to the high stiffness of the device, we observe that the displacement in any of the three principal directions is very small. The largest displacement (~ 56 μm) appears in the mobile block where the right jaw is attached. The maximum stress (~ 160 MPa) is found at the steel jaws, and is well below the yield stress of the material (700 MPa).

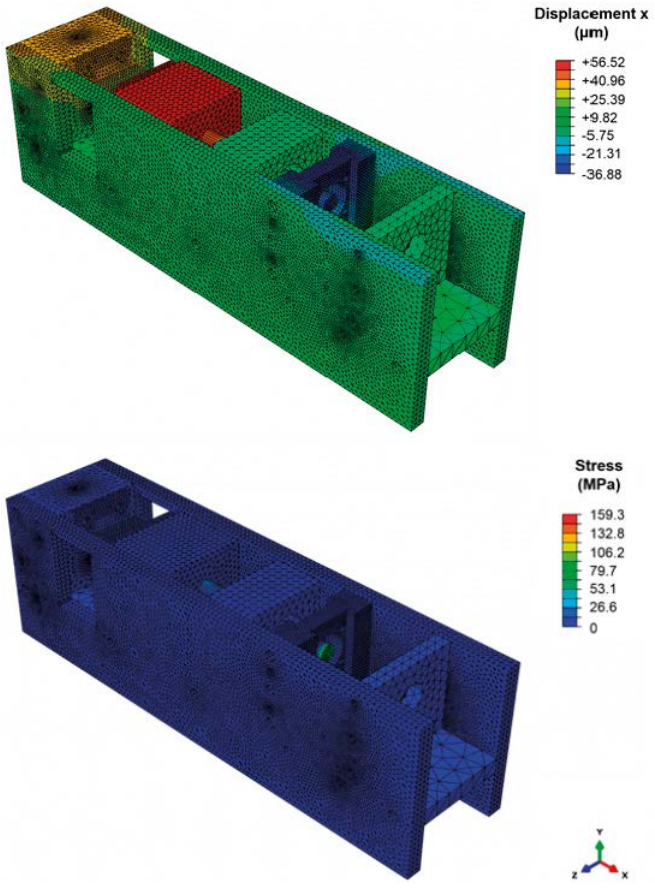

Figure 2-6. *Modeling results of the displacement (top) and von Mises stress (bottom) distributions at the maximum compressive load (25 kN) applied during the stiffness assessment of the pCT experimental device.*

Testing procedures

*p*CT tests were executed according to the guidelines indicated by Muñoz-Ibáñez et al. (2020) and they are summarised in Table 2-4.

As described above, for fracture toughness investigations in rocks, two testing levels are commonly reported in the literature (Ouchterlony 1988). Although the features and characteristics of the testing equipment are compatible with level II, the interpretation of tests will be made based on level I consideration after a careful assessment of its applicability to the tested samples (see next section).

Table 2-4. *p*CT testing procedure.

Step	Description
1	Digital photos are taken of the specimen before the mechanical testing. The sample is equipped with a 6 mm-diameter magnet (which is glued with cyanoacrylate) that is used to attach the acoustic emission sensor.
2	The specimen is placed on the positioning cradle and then lifted until the steel jaws fit into the groove. The height of the cradle is manually controlled using a positioning spindle.
3	The verticality of the specimen is checked using a self-levelling cross-line laser.
4	AE sensors are mounted on the surface of the specimen and a digital camera is placed in front of it to record the experiment. Load and displacement channels are zeroed at this time.
5	The stress (load) and LPD (linear displacement sensor) measurement channels are zeroed in the data acquisition software.
6	The beginning of the test is concurrent to recording. Recorded data includes load, load point displacement (LPD), AE activity, etc. The test is executed in displacement-control mode at a constant rate of 0.1 mm/min (0.0017 mm/s).
7	The test is stopped manually (switch off) after peak load has been observed and the applied force has fallen to a level of ~5 % of peak load.
8	Digital photos are taken of the specimen upon completion of each test.
9	The testing device is disassembled and carefully cleaned for the next test.

Data processing

Following Muñoz-Ibáñez at al. (2020), the computation of K_{IC} (in MPa $m^{1/2}$) for the *p*CT testing method can be performed according to the following equation:

$$K_{IC}^{pCT} = Y'_{pCT}\sigma_{max}\sqrt{\pi a}$$

where σ_{max} is the applied stress at the critical load ($\sigma_{max} = P_{max}/bB$; in Pa) and B the thickness of the specimen (in m). In order to compute the specific non-dimensional stress intensity factor Y'_{pCT}, these authors provide the following equation:

$$Y'_{pCT} = C_0 + C_1\left(\frac{a}{b}\right) + C_2\left(\frac{a}{b}\right)^2 + C_3\left(\frac{a}{b}\right)^3 + C_4\left(\frac{a}{b}\right)^4$$

The coefficients C_i (i = 0 to 4) to compute the stress intensity factor are indicated in Table 2-5.

Table 2-5 Coefficients for the computation of the specific non-dimensional stress intensity factor Y'_{pCT} of the *p*CT fracture toughness testing method.

D (mm)	C_0	C_1	C_2	C_3	C_4
38	10.278	−24.069	82.329	−136.670	127.890
50	12.651	−47.054	158.720	−247.170	185.22
100	15.341	−74.551	260.030	−404.520	273.19

2.4.3 Acoustic emission monitoring

Acoustic emission (AE) monitoring is not required for fracture toughness testing although, as a complementary non-destructive technique, provides with useful information about fracturing like crack initiation, propagation and coalescence. For this research we conducted AE measurements with the aid of a multichannel AMSY-6 AE data acquisition system (*Vallen Systeme GmbH*) equipped with 8 ASIP-2 boards (2 channels per board) with capability of managing up to 16 independent signals. The AE transducers used were miniature *Vallen* VS700-D sensors (frequency range: 150–800 kHz; peak frequency: 600–800 kHz) whose main dimensions are 6.3 mm-diameter and 10 mm-length. They were located at different distances of the starter notch.

Continuous waveforms were recorded at a sampling rate of 10 MHz and, in order to eliminate unwanted frequency components (associated with environmental or system noises) we set up a band-pass filter (95–850 kHz) and signal threshold level of 40 dB.

At the time of fracture toughness testing, one AE sensor was attached to each sample using a 6 mm-diameter, 3 mm-height magnet that was glued with a thin layer of cyanoacrylate glue. The face of the magnet in contact with the transducer was covered with a touch of *Multi-Silicone* grease (*OKS* 1110) to improve the acoustic coupling (ASTM 1997).

The raw AE signals were enhanced with *Vallen* AEP5 preamplifiers set with 34 dB gain. With this AE setup, time-resolved AE parameters recorded in real-time included signal peak amplitude (A), counts, event duration, rise time, and energy (E_{AE}). E_{AE} is computed in aJ (10^{-18} J) from the root-mean square of the integral of the squared voltage signal divided by a reference resistance (10 kΩ in the AE system used) over the duration of the recorded AE transient (Vallen 2017). Other properties such as average frequency (AF), rise angle (RA) and different cumulative values were computed afterwards.

AE data analysis

A number of criteria based on the investigation of cracking modes have been published to characterise damage in engineering materials. For the present investigation, we focus on the parameter-based methodology proposed by the *Federation of Construction Materials Industries of Japan* (JCMS-III B5706 2003, Ohno and Ohtsu 2010), later incorporated as recommendation for concrete materials by the RILEM (Ohtsu 2010). This has been further improved for its application to selected rocks by Du et al. (2020).

In the case of RILEM (Ohtsu 2010), the methodology is grounded on an experimental database of four-point bending and direct shear tests performed with concrete-type materials, and indicates that it is possible to discriminate among tensile, shear or mixed-mode (tensile-shear) cracks according to the ratio existing between the average frequency (AF = counts/duration) and rise angle (RA = rise time/peak amplitude) obtained from AE testing:

- If the AF *vs.* RA ratio is >0.1 Hz·V/s, the corresponding AE events are considered to be originated by tensile stresses.
- If the AF *vs.* RA ratio is <0.1 Hz·V/s would correspond to crack shearing.
- Those events with a AF *vs.* RA ratio of ~0.1 Hz·V/s are likely to be occasioned by a mix-mode of cracking.

In the case of Du et al. (2020) the classification is based on the results of a series of indirect tensile (Brazilian) and modified shear tests carried out with three different types of rocks: Granite, marble and sandstone. According to these authors, the transition between tensile and shear events is given by the relation AF (kHz) = 11RA (10^5 μs/V) + 60 for granite-like rocks.

2.5 Assessment of the validity of fracture toughness test results

The assessment of the validity of fracture toughness results based on Level I testing requires the fulfilment of some acceptability criteria that have not been yet sufficiently established for rocks. Furthermore, both the SCB and *p*CT methods do not include any specific procedure for the non-linearity corrections inherent to Level II testing. In order to elaborate a minimum acceptability criterion, we have considered the use of the *compliance (or 5 % secant)* method which is covered, among others, by the standard ASTM E399-12 (ASTM 2012).

The secant compliance method seeks to verify the applicability of the linear elastic fracture mechanics (or LEFM) postulates. A 5 % secant line with a slope equal to 95 % of the initial elastic loading slope is normally used to determine P_5 (or P_Q). This slope would correspond approximately with the load required to generate a ~2 % (or less) apparent crack extension.

2.5.1 Linearity criterion

Figure 2-7 illustrates the application of the secant compliance method to the linearity criterion to one of the 101057 rock specimens tested using the *p*CT methodology. The procedure for its application is as follows:

- A linear best fit line is computed to the linear loading segment of the experimental P-CMOD curve to determine the initial compliance (Q). This is given by the reciprocal of the slope of line (AB).
- A second line (AB') is draw with a compliance 5 % greater than that of line (AB).

The experimental data provides with a P_{max} value (maximum load that the specimen was able to sustain during the test) and the intersection of the (AB') line with the experimental curve identify the so-called conditional load (P_Q). Based on these references it is possible to compute a P_{max}/P_Q ratio that, if smaller than 1.10 supports the applicability of the LEFM hypotheses. In case it was larger, then an elasto-plastic approach (Level II) would be required to characterise K_{IC} as a material property. In the case of the example illustrated in Figure 2-7 the P_{max}/P_Q ratio is 1.04 what makes possible the computations associated with Level I fracture toughness testing.

The standard ASTM E399-12 (ASTM 2012) also specifies the situations in which P_{max} is located between the (AB) and (AB') curves and when it lays ahead of the (AB') line. In the first case, the computation of K_{IC} can be directly performed based on the P_{max} value while in the second the prescribed value to use is P_Q. Based on that, what we obtain in each case is a conditional value (K_Q, derived from P_Q) or the true mode I fracture toughness K_{IC} (when using P_{max}).

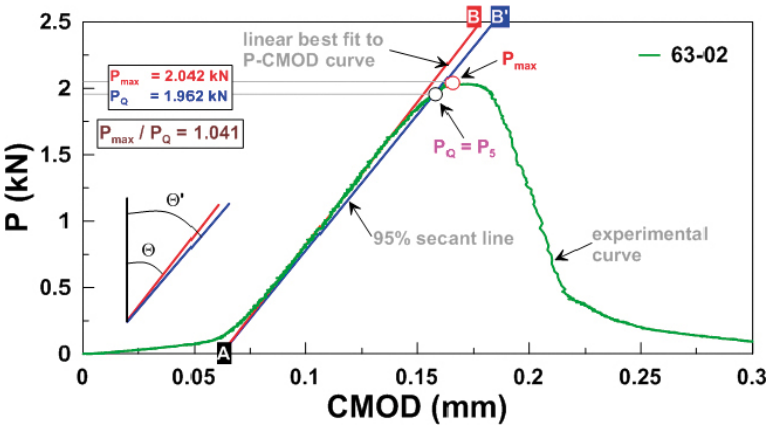

Figure 2-7. *Experimental results corresponding a pCT test used to verify the linearity criterion of the compliance method. See text for explanation Notes: P = applied horizontal load; P_{max} = maximum load; P_Q = conditional load; CMOD = crack mouth opening displacement (≡ load point displacement in the pCT test); Θ = compliance angle; Θ' = compliance angle of the 95 % P-CMOD slope.*

2.5.2 Plane-strain criterion

The standard ASTM E399-12 (ASTM 2012) pays attention to the fulfilment of plane-strain conditions to determine a K_{IC} value that can be considered as a true material property. To this respect, sample thickness is a key property as it affects how the plastic domain around the crack tip (or fracture process zone, FPZ) is fully developed within the body of the specimen (i.e., its outer boundaries are not strained) or it interacts with them.

For the SCB method, the ISRM suggests that the minimum diameter (D) of the tested sample should keep in line with the following relationship:

$$\boldsymbol{D \geq 2(K_{IC}/T)^2}$$

where T represents tensile strength. This expression is derived from theoretical considerations on the size of the fracture process zone (L_{FPZ}), which is considered to be proportional to the square ratio of K_{IC} and T:

$$\boldsymbol{L_{FPZ} \propto (K_{IC}/T)^2}$$

The application of this criterion is not straightforward because, although we may have an accurate assessment of T, the computation of K_{IC} requires testing of specific specimens. Although the recommended thickness of SCB and *p*CT specimens are given in the corresponding literature sources it may be worth to consider whether these dimensions are adequate for the 101057 rock.

Due to the impracticability of conducting a specific survey addressing the thickness-dependence of K_{IC} in this rock we have considered an *ex post* assessment. That is, based on the K_{IC} values computed, the known value of T and the corresponding thickness of the tested specimens it is possible to assess L_{FPZ} whose dimension is then compared with the thickness of the samples. If L_{FPZ} turns out to be larger than the corresponding thickness, then the plane strain condition can be assumed to be compromised and the K_{IC} value obtained inaccurate.

A number of researchers have considered different approaches to compute the length of FPZ (Dutler et al. 2018 and references therein). Worth mentioning among them are the basic model of Irwin ($L_{FPZ,I}$), the strip-yield uniform traction model ($L_{FPZ,SU}$) and the strip-yield linear traction model ($L_{FPZ,ST}$). The expressions used to compute L_{FPZ} for each of them are the following:

$$\boldsymbol{L_{FPZ,I} = \frac{1}{\pi}\left(\frac{K_{IC}}{T}\right)^2} \qquad \boldsymbol{L_{FPZ,SU} = \frac{\pi}{8}\left(\frac{K_{IC}}{T}\right)^2} \qquad \boldsymbol{L_{FPZ,ST} = \frac{9\pi}{32}\left(\frac{K_{IC}}{T}\right)^2}$$

2.6 Statistic treatment and data reduction

Upon test and experimental data processing completion, results were assessed with the aim of determining its statistical significance and to investigate representativeness, repeatability and comparability of the two testing methods.

The statistical analysis was conducted with the aid of the free software *Past* 4.04 (Hammer et al. 2001). This is a powerful software for scientific data analysis, with functions for data manipulation, plotting, univariate and multivariate statistics, ecological analysis, time series and spatial analysis, morphometrics and stratigraphy. Although *Past* was initially conceived for use of the paleontological community, along the past 20 years it has grown into a comprehensive statistics package used in many fields of the life and earth sciences, engineering, and economics.

The experimental data obtained in this study was assessed based on a systematic approach. The results associated with each testing method (SCB and *p*CT) were separated for the analysis. Then, a normality test (Shapiro-Wilk) was performed with each group of data. This returns a test statistic W, (which lies between 0 and 1 and is small for non-normal samples) and a probability p, value. The Shapiro-Wilk test is adequate for small sample populations (<50 originally) although it can be safely used up to sizes of ~ 2 000 samples. If the two group of samples were statistically found to conform to normal distributions, then their corresponding mean values were checked for semblance based on a one-way analysis of variance (ANOVA) and the non-parametric Mann-Whitney pairwise test. For this (and the other tests/analyses conducted) we used a significance level of 95 % (a = 0.05) so that the rejection of the null hypothesis (H_0) can be verified if the p-level is below this significance.

3 Results

Table 3-1 and Table 3-2 summarise the geometrical properties of the tested specimens. The meaning and definitions are given in Figure 2-3 and Figure 2-5 and Section 2.4. Table 3-3 presents the results of the tests which are discussed in more detail in the following sections.

Table 3-1 Geometrical properties of the specimens of rock RFM029 used in the SCB fracture toughness determinations.

Sample	Test	D (mm)	B (mm)	a (mm)	S (mm)
100-1a	SCB	99.36	48.62	27.02	79.49
100-1b	SCB	99.36	48.62	27.02	79.49
100-3a	SCB	99.11	49.79	27.02	79.29
100-3b	SCB	99.11	49.79	27.02	79.29
100-8a	SCB	98.86	44.71	27.02	79.09
100-8b	SCB	98.86	44.71	27.02	79.09

Notes: D = diameter; B = thickness; a = starter notch length; S = span length (see Figure 2-3).

Table 3-2. Geometrical properties of the specimens of rock RFM029 used in the *p*CT fracture toughness determinations.

Sample	Test	D (mm)	B (mm)	a (mm)	G_d (mm)	G_w (mm)	b (mm)	a/b (–)
63-1	*p*CT	64.19	31.58	15.41	6.52	10.0	57.67	0.27
63-2	*p*CT	64.22	30.75	14.41	6.14	10.0	58.08	0.25
63-3	*p*CT	64.22	31.94	15.15	6.56	10.0	57.66	0.26
63-6	*p*CT	64.14	32.63	15.12	6.62	10.0	57.52	0.26
63-11	*p*CT	64.05	30.91	15.62	6.23	10.0	57.82	0.27
63-12	*p*CT	64.06	29.91	15.76	5.92	10.0	58.14	0.27

Notes: D = diameter; B = thickness; a = starter notch length; G_d = groove depth; G_w = groove width; b = distance from the base of the groove to the bottom of the specimen (see Figure 2-5).

3.1 Acceptability of fracture toughness results

It was indicated earlier that, in the absence of specific criteria or recommendations about the acceptability of fracture toughness test results in rocks, we have conducted a two-step check based on the considerations made in the standard ASTM E399-12 (ASTM 2012) about plane-strain fracture toughness of metallic materials: a) Linearity compliance check based on the 5 % secant line slope method; and b) Plane-strain compliance check based on the estimated size of the fracture process zone.

Table 3-3 shows the results of the assessment of the P_{max}/P_Q ratio for all the tested rocks and methods. Graphical information is also provided in Appendix 2. We see that, irrespective of the testing method and with the only exception of the *p*CT sample 63-6, this ratio is below the 1.10 threshold value what would confirm the applicability of LEFM formulations for the computation of K_{IC} in Level I testing. Sample 63-6 shows a P_{max}/P_Q ratio of 1.11, slightly above the reference value. It is debatable whether such small departure from the reference is significant (remember that this value is based on metals testing, not rocks) and that should be taken into account.

Table 3-3. Fracture toughness test results of the specimens of rock RFM029.

Sample	Test	P_{max} (kN)	P_Q (kN)	P_{max}/P_Q (–)	K_{IC} (MPa $m^{1/2}$)	K_Q (MPa $m^{1/2}$)
*100-1a**	*SCB*	*2.190*	*2.118*	*1.034*	*0.97*	*0.94*
*100-1b**	*SCB*	*2.236*	*2.162*	*1.034*	*0.99*	*0.96*
100-3a	SCB	4.041	3.935	1.027	1.76	1.71
100-3b	SCB	3.128	2.993	1.045	1.36	1.30
100-8a	SCB	4.073	4.007	1.016	1.99	1.96
100-8b	SCB	2.357	2.248	1.048	1.15	1.10
*63-1**	*pCT*	*1.493*	*1.366*	*1.093*	*1.38*	*1.26*
63-2	*p*CT	2.042	1.962	1.041	1.87	1.80
63-3	*p*CT	1.780	1.716	1.037	1.61	1.56
63-6	*p*CT	1.711	1.542	1.110	1.52	1.37
63-11	*p*CT	1.942	1.857	1.046	1.84	1.76
63-12	*p*CT	1.672	1.575	1.062	1.63	1.54

Notes: P_{max} = maximum load at failure; P_Q = conditional load level; K_{IC} = fracture toughness; K_Q = conditional fracture toughness; * = samples not included in the statistical assessment after the acceptability checks.

The P_{max} value of all the SCB samples is located over the initial elastic loading slope (AB) while in the case of the *p*CT samples, that value is on the right of the 5 % secant slope line (AB'). Based on the previous information, in line with the indications of the standard ASTM E399-12 (ASTM 2012), P_{max} has been used with the SCB samples and P_Q with the *p*CT ones to perform toughness computations.

When analyzing in more detail the experimental curves, we observe that only the *p*CT specimen 63-1 shows P_{max} at the left of the (AB) line. This unusual behavior joined to the facts that P_Q lays in the post-peak loading region and the small compliance angle (compared with the rest of samples in the group) make us to consider its exclusion of further assessments.

Table 3-4 summarises the results of theoretical computations about the length of the inelastic fracture process region around the crack tip (or FPZ) of the tested specimens. This represents a transition domain between the propagating macro-crack and its far surroundings, which is assumed to be continuous (i.e. not fractured) at micro-scale.

Table 3-4 Theoretical length of the fracture process associated with the fracture toughness tests (SCB and *p*CT) of rock RFM029 zone according to the models of Irwin ($L_{FPZ,I}$), strip-yield uniform traction ($L_{FPZ,SU}$) and strip-yield linear traction ($L_{FPZ,ST}$).

Sample	Test	$L_{FPZ,I}$ (mm)	$L_{FPZ,SU}$ (mm)	$L_{FPZ,ST}$ (mm)
100-1a	*SCB*	*1.52*	*1.88*	*4.22*
100-1b	*SCB*	*1.58*	*1.96*	*4.40*
100-3a	SCB	4.99	6.16	13.86
100-3b	SCB	2.99	3.69	8.30
100-8a	SCB	6.37	7.85	17.67
100-8b	SCB	2.13	2.63	5.92
63-1	*pCT*	*3.06*	*3.78*	*8.50*
63-2	*p*CT	5.63	6.94	15.62
63-3	*p*CT	4.19	5.17	11.64
63-6	*p*CT	3.72	4.59	10.33
63-11	*p*CT	5.45	6.72	15.13
63-12	*p*CT	4.30	5.31	11.95

Note: Data used to make the computations were derived from the tests and the average tensile strength of rock RFM029 reported in Table 2-1* = samples not included in the statistical assessment after the acceptability tests.

The computations have been performed using three theoretical models that have been described in detail by Dutler et al. (2018). Based on their conclusions, the size of FPZ is underestimated when this is computed using Irwin's and strip-yield uniform traction models and it is overestimated when the strip-yield linear traction model is considered. Accepting their conclusions as valid, these provide with minimum and maximum bounds for the extent of the FPZ that can be compared with specimen thickness (~50 mm for SCB and ~30 mm for *p*CT). We observe that, in both cases, the length of FPZ is neatly below the thickness of the sample what would confirm the compliance with the plane-strain test requirement in both cases.

3.2 Fracture toughness test results

Figure 3-1 summarise the experimental results of the fracture toughness test survey conducted with specimens of rock 101057 and Table 3-5 summarises the statistical assessment of the experimentally obtained K_{IC} values previously shown in Table 3-3. Appendix 2 compiles the corresponding photographic survey and more detailed graphical representation and analysis of the experiments.

It is interesting to observe that, with the exception of sample 63-1, the compliance angle of all the *p*CT specimens is consistent and comparable. This anomaly is likely related with the slippage of one of the loading jaws with respect the contact surface with the groove of the specimen. Although this effect affects the magnitude of displacements, should not affect loads. In any case, in the data screening stage, it was decided to discard the results associated with this sample.

With respect the SCB samples, we observe that the compliance angle of samples 100-1a and 100-1b is significantly smaller than the rest of the samples. Similar happens with the corresponding P_{max} values. This behavior perhaps suggests inhomogeneity within the tested samples. In fact, sample 100-1a is characterised by the presence of centimeter-size clumps of biotite crystals likely reducing its mechanical performance. Likewise, sample 100-1b has grain crystals whose size is large compared with the dimensions of the ligament area. Because these are not representative features of the matrix of the tested rocks, these two samples were discarded from the assessment.

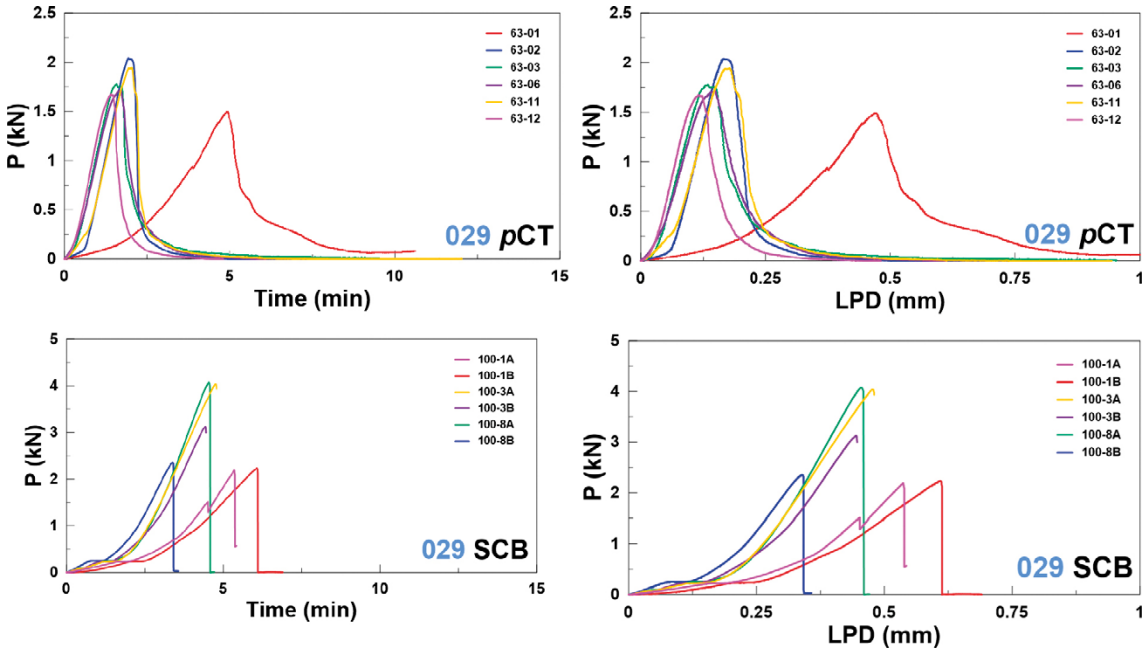

Figure 3-1. *Experimental curves corresponding to pCT (top) and SCB (bottom) tests performed with specimens of rock RFM029. Note: LPD = load point displacement.*

Table 3-5 Summary statistics of the K_{IC} (K_Q in the case of the *p*CT tests) obtained in the fracture toughness test specimens of rock RFM029.

Test	SCB	*p*CT	All
n	5	4	9
Min_i	1.15	1.37	1.15
Max_i	1.99	1.76	1.99
Σ_i	8.06	6.23	14.29
Ave	1.61	1.56	1.59
SE_i	0.15	0.08	0.09
σ_i^2	0.119	0.025	0.070
σ_i	0.345	0.160	0.265
Med_i	1.76	1.55	1.56
Q_1	1.26	1.41	1.37
Q_3	1.90	1.71	1.78
Skew	−0.513	0.280	−0.185
Kurt	−1.696	1.466	−0.657
GM_i	1.58	1.55	1.57
CV_i	21.424	10.251	16.666
W_i	0.926	0.963	0.965
p(0.05)	0.566	0.797	0.853
A_i	0.284	0.243	0.231
p(0.05)	0.467	0.527	0.722

Notes: n = number of samples; Min_i = minimum sample value; Max_i = maximum sample value; Σ_i = sum; Ave = mean; SE_i = standard error of the mean; σ_i^2 = variance; σ_i = standard deviation; Med_i = median; Q_1 = 1st quartile (25 %); Q_3 = 3rd quartile (75 %); Skew = skewness; Kurt = kurtosis; GM_i = geometric mean; CV_i = coefficient of variation; W_i = Shapiro-Wilk test; A_i = Anderson-Darling test; p(0.05) = normal distribution probability for a significance level of 95 %

The statistical assessment has focused on the K_{IC} value and that has been derived from P_{max} (in the case of the SCB test) and P_Q (in the case of the *p*CT test). This differentiation obeys to the considerations made earlier in relation with the acceptability criteria discussed in Section 3.1. The Shapiro-Wilk test indicates that both SCB and *p*CT groups of specimens conform to a normal distribution. Furthermore, the Mann-Whitney test results obtained after a one-way ANOVA analysis of the mean values of both groups suggest that both populations are comparable (p=0.806 for a significance level a=0.05). The average K_{IC} value of rock RFM029 is 1.59 ± 0.09 MPa $m^{1/2}$.

3.3 Acoustic emission

Acoustic emission (AE) determinations were conducted as a complementary technique to improve the characterization of the mechanical processes occurring during the execution of fracture toughness tests. A summary of the results associated with each test is presented in Appendix 2. A detailed assessment of AE results is out of the scope of the present report and only some general ideas about the role of AE measurement in SCB and *p*CT testing will be given.

In general, the AE sensitivity of SCB tests is lower than in the *p*CT ones. That translates into lower number of counts and a lower capacity to identify significant mechanic events during the test. Most of the AE activity in the SCB tests concentrates in the final stages although the cumulative curves (energy, counts) tend to display a slope rupture at the onset of the initial elastic stage. A second major step occurs slightly in advance to P_{max}, suggesting perhaps the initiation of subcritical crack growth and coalescence.

The AE records of *p*CT tests provides with much more significant information. In nearly all the monitored tests the number of counts is so large that, at some points, the data acquisition system become saturated (at the onset of cracking). However, most of the recorded information is continuous and allows for a more detailed analysis of the cracking processes. Like in the SCB case, the cumulative counts and energy curves display slope rupture points that are clearly connected with the loading curves. Furthermore, the indicator RA and AF parameters show distinct evolutions during the test. For instance, before peak load, RA is consistent with higher amplitude events with shorter rise times while after peak load the same property corresponds to lower amplitudes and bigger rise times. The maximum of RA is attained at the time of cracking. On the other hand, the AF parameter shows lower counts of higher average duration at the beginning of the elastic slope attaining a maximum at peak load. Then the AE record tends to have a higher count number of shorter duration. The combined behaviour of the AF and RA parameters allow to conjecture that, in the *p*CT tests, the mechanics of fracturing before peak load are dominated by tensile processes while there is an increase of shear or mixed tensile/shear phenomena after peak load.

The peak frequency record of *p*CT tests also shows interesting properties and it is worth to identify moments in which certain frequency bands start to develop. For instance, the 350 kHz frequency band starts to develop at the load/time conditions consistent with the first onset of subcritical crack growth (i.e., after the purely elastic region).

4 Conclusions

The fracture toughness of twelve samples from rock boulders at the surface within domain RFM029 in Forsmark has been determined using the ISRM's semi-cylinder bending (SCB) suggested method (6 samples) and a newly developed alternative known as the pseudo-compact tension (*p*CT) method (6 samples). The methodology to conduct both types of tests is presented in detail, as well as a procedure for the assessment of the validity of the fracture toughness results in Level I testing. This methodology evaluates the linearity condition (for the application of LEFM equations) and the compliance of the grown crack within a plane-strain framework.

With the exception of 1 sample (which was excluded from later analyses), all the results were acceptable in terms of the validity criteria applied. However, two more SCB samples have been also discarded due to their perceived not representativeness when compared with more typical rock matrix specimens of the studied lithology.

The statistical assessment of results shows that the results of both types of testing methods conform to normal distribution functions and, when their mean values are compared, they are similar considering a 5 % level of significance. Based on that, the average fracture toughness of the tester granite to granodiorite (101057) is 1.59 ± 0.09 MPa $m^{1/2}$ (Table 3-5).

Acoustic emission results illustrate some relevant features about the mechanics of cracking of the tested samples. However, the AE data associated with the *p*CT tests incorporates a more significant wealth of information than the one corresponding to SCB.

References

SKB's (Svensk Kärnbränslehantering AB) publications can be found at www.skb.com/publications.

ABAQUS, 2014. ABAQUS Version 6.14/analysis user's guide. Providence: Dassault Systemes Simulia Corporation.

ASTM, 1997. E650-97: Standard guide for mounting piezoelectric acoustic emission sensors. West Conshohocken, PA: ASTM International.

ASTM, 2012. E399-12: Standard test method for linear-elastic plane-strain fracture toughness K_{IC} of metallic material. West Conshohocken, PA: ASTM International.

ASTM, 2018. E2309-18: Standard practices for verification of displacement measuring systems and devices used in material testing machines. West Conshohocken, PA: ASTM International.

Delgado-Martín J, Alejano R L, 2021. Sample size effects on intact granitic rocks through uniaxial compressive and tensile testing and geophysical measurements. SKB P-20-25, Svensk Kärnbränslehantering AB.

Du K, Li X, Tao M, Wang S, 2020. Experimental study on acoustic emission (AE) characteristics and crack classification during rock fracture in several basic lab tests. International Journal of Rock Mechanics and Mining Sciences 133, 104411. doi:10.1016/j.ijrmms.2020.104411

Dutler N, Nejati M, Valley, B, Amann F, Molinari G, 2018. On the link between fracture toughness, tensile strength, and fracture process zone in anisotropic rocks. Engineering Fracture Mechanics 201, 56–79.

Fowell R J, 1995. Suggested method for determining mode I fracture-toughness using cracked chevron notched Brazilian disc (CCNBD) specimens. International Journal of Rock Mechanics and Mining Sciences & Geomechanical Abstracts 32, 57–64.

Hammer Ø, Harper D A T, Ryan P D, 2001. Past: Paleontological statistics software package for education and data analysis. Paleontologia Electronica 4. Available at: https://palaeo-electronica.org/2001_1/past/past.pdf

JCMS-III B5706, 2003. Monitoring method for active cracks in concrete by acoustic emission. Federation of Construction Materials Industry of Japan. (In Japanese.)

Kuruppu M D, Obara Y, Ayatollahi M R, Chong K P, Funatsu T, 2014. ISRM-suggested method for determining the mode I static fracture toughness using semi-circular bend specimen. Rock Mechanics and Rock Engineering 47, 267–274.

Muñoz-Ibáñez A, Delgado-Martín J, Costas M, Rabuñal-Dopico J, Alvarellos-Iglesias J, Canal-Vila J, 2020. Pure mode-I fracture toughness determination in rocks using a pseudo-compact tension (*p*CT) test approach. Rock Mechanics and Rock Engineering 53, 3267–3285.

Ohno K, Ohtsu M, 2010. Crack classification in concrete based on acoustic emission. Construction and Building Materials 24, 2339–2346.

Ohtsu M, 2010. Recommendation of RILEM TC 212-ACD: Acoustic emission and related NDE techniques for crack detection and damage evaluation in concrete: Test method for classification of active cracks in concrete structures by acoustic emission. Materials and Structures 43, 1187–1189.

Ouchterlony F, 1988. Suggested methods for determining the fracture toughness of rock. International Journal of Rock Mechanics and Mining Sciences & Geomechanical Abstracts 25, 71–96.

Ouchterlony F, 1989. Fracture toughness testing of rock with core based specimens, the development of an ISRM standard. In Mihashi H, Takahashi H (eds). Fracture Toughness and Fracture Energy. Rotterdam: Balkema, 231–251.

SKB, 2013. Site description of the SFR area at Forsmark at completion of the site investigation phase. SDM-PSU Forsmark. SKB TR-11-04, Svensk Kärnbränslehantering AB.

UNE, 2018. UNE-EN ISO 7500-1:2018: Metallic materials – Calibration and verification of static uniaxial testing machines – Part 1: Tension/compression testing machines – Calibration and verification of the force-measuring system. Madrid: UNE.

Vallen, 2017. AMSY-6 Operation manual. Icking, Germany: Vallen Systeme GmbH.

Appendix 1

Calibration and standard certificates

Table A1- 1 Calibration certificate of force corresponding to the internal motor encoder of the equipment used to perform the SCB tests.

servosis Testing Machines
comercial@servosis.com
SERVOSIS S.L. - Laboratorio de Calibración
C/ Fuentevieja, 8-10. Pol Ind La Estación
28320 Pinto - Madrid – Spain
Tlf +34 91 691 68 61

RESULTADOS

Escala calibrada: 50 kN
Sentido: Compresión
Resolución: 0,001 kN

Fuerza nominal (kN)	Lectura 1 (kN)	Lectura 2 (kN)	Lectura 3 (kN)	Lectura 4 (kN)	Media (kN)
10,000	10,001	9,999	10,009		10,003
15,000	14,995	14,981	14,990		14,989
20,000	19,996	19,926	19,937		19,953
25,000	24,904	24,914	24,906		24,908
30,000	29,925	29,896	29,899		29,907
35,000	34,983	34,899	34,906		34,929
40,000	39,864	39,890	39,893		39,882
45,000	44,835	44,805	44,830		44,823
47,500	47,312	47,320	47,309		47,314
Vuelta a cero:	0,040	0,021	0,019		

Punto de Calibración	Error relativo de indicación (q)	Error relativo de repetibilidad (b)	Resolución relativa (a)
10,000	-0,03%	0,10%	0,01%
15,000	0,08%	0,09%	0,01%
20,000	0,24%	0,35%	0,01%
25,000	0,37%	0,04%	0,00%
30,000	0,31%	0,10%	0,00%
35,000	0,20%	0,24%	0,00%
40,000	0,30%	0,07%	0,00%
45,000	0,39%	0,07%	0,00%
47,500	0,39%	0,02%	0,00%

Error relativo de cero (f_0):	Lectura 1	Lectura 2	Lectura 3
	0,084%	0,044%	0,040%

Clase 1 para todo el rango calibrado. La Clase se ha determinado según EN-7500-1 Tabla 2.

La Incertidumbre asociada para todo el rango es del 0,20 %. Esta incertidumbre ha sido calculada multiplicando la incertidumbre típica de medida por el factor de cobertura k=2, que para una distribución normal corresponde a una probabilidad de cobertura de aproximadamente el 95%. La incertidumbre típica de medida se ha determinado según Norma 7500-1:2018 Anexo C.

Table A1- 2 Calibration certificate of displacement corresponding to the internal motor encoder of the equipment used to perform the SCB tests.

comercial@servosis.com

SERVOSIS S.L. - Laboratorio de Calibración
C/ Fuentevieja, 8-10. Pol Ind La Estación
28320 Pinto - Madrid – Spain
Tlf +34 91 691 68 61

6- RESULTADOS

Escala calibrada: 200 mm.
Sentido: Incremento.
Resolución: 0,01 mm.

Desplazam nominal	Lectura 1	Lectura 2	Media
(mm)	(mm)	(mm)	(mm)
10,000	9,981	9,983	9,982
20,000	19,980	19,988	19,984
40,000	39,991	39,989	39,990
60,000	59,981	59,975	59,978
80,000	79,961	79,959	79,960
100,000	99,969	99,971	99,970
120,000	119,932	119,936	119,934
140,000	139,951	139,948	139,950
160,000	159,981	159,989	159,985
180,000	179,998	179,953	179,976

	Resolución		Error		
Punto de Calibración	Absoluta (mm)	Relativa (%)	Absoluto (mm)	Relativo (%)	Error de repetibilidad
10,000	0,0010	0,01%	-0,018	-0,18%	0,02%
20,000	0,0010	0,01%	-0,016	-0,08%	0,04%
40,000	0,0010	0,00%	-0,010	-0,02%	0,01%
60,000	0,0010	0,00%	-0,022	-0,04%	0,01%
80,000	0,0010	0,00%	-0,040	-0,05%	0,00%
100,000	0,0010	0,00%	-0,030	-0,03%	0,00%
120,000	0,0010	0,00%	-0,066	-0,06%	0,00%
140,000	0,0010	0,00%	-0,050	-0,04%	0,00%
160,000	0,0010	0,00%	-0,015	-0,01%	0,01%
180,000	0,0010	0,00%	-0,024	-0,01%	0,03%

Clase A según ASTM E2309 para todo el rango calibrado.

La Incertidumbre asociada para todo el rango es de 0,19%. Esta incertidumbre ha sido calculada multiplicando la incertidumbre típica de medida por el factor de cobertura k=2, que para una distribución normal corresponde a una probabilidad de cobertura de aproximadamente el 95%. La incertidumbre típica de medida se ha determinado según ASTM E2309-16 Apéndice X2.

Table A1.3. Calibration certificate of displacement corresponding to the magnetorestrictive transducer of the equipment used to perform the SCB tests.

SERVOSIS S.L. - Laboratorio de Calibración
C/ Fuentevieja, 8-10. Pol Ind La Estación
28320 Pinto - Madrid – Spain
Tlf +34 91 691 68 61
comercial@servosis.com

6- RESULTADOS

Escala calibrada: 200 mm.
Sentido: Incremento.
Resolución: 0,01 mm.

Desplazam nominal	Lectura 1	Lectura 2	Media
(mm)	(mm)	(mm)	(mm)
10,000	9,982	9,983	9,983
20,000	20,001	20,001	20,001
40,000	40,019	40,020	40,020
60,000	60,071	60,069	60,070
80,000	80,068	80,060	80,064
100,000	100,103	100,100	100,102
120,000	120,131	120,133	120,132
140,000	140,162	140,149	140,156
160,000	160,194	160,192	160,193
180,000	180,209	180,210	180,210

	Resolución		Error		
Punto de Calibración	Absoluta (mm)	Relativa (%)	Absoluto (mm)	Relativo (%)	Error de repetibilidad
10,000	0,0010	0,01%	-0,018	-0,18%	0,01%
20,000	0,0010	0,01%	0,001	0,01%	0,00%
40,000	0,0010	0,00%	0,020	0,05%	0,00%
60,000	0,0010	0,00%	0,070	0,12%	0,00%
80,000	0,0010	0,00%	0,064	0,08%	0,01%
100,000	0,0010	0,00%	0,102	0,10%	0,00%
120,000	0,0010	0,00%	0,132	0,11%	0,00%
140,000	0,0010	0,00%	0,155	0,11%	0,01%
160,000	0,0010	0,00%	0,193	0,12%	0,00%
180,000	0,0010	0,00%	0,209	0,12%	0,00%

Clase A según ASTM E2309 para todo el rango calibrado.

La Incertidumbre asociada para todo el rango es de 0,19%. Esta incertidumbre ha sido calculada multiplicando la incertidumbre típica de medida por el factor de cobertura k=2, que para una distribución normal corresponde a una probabilidad de cobertura de aproximadamente el 95%. La incertidumbre típica de medida se ha determinado según ASTM E2309-16 Apéndice X2.

Appendix 2

Experimental results and photograph survey

Figure A2-1. *Sample 101057 100-1a before (left) and after (middle and right) conducting a SCB test. The K_{IC} value obtained was of 0.97 MPa $m^{1/2}$ obtained for a maximum load of 2.19 kN.*

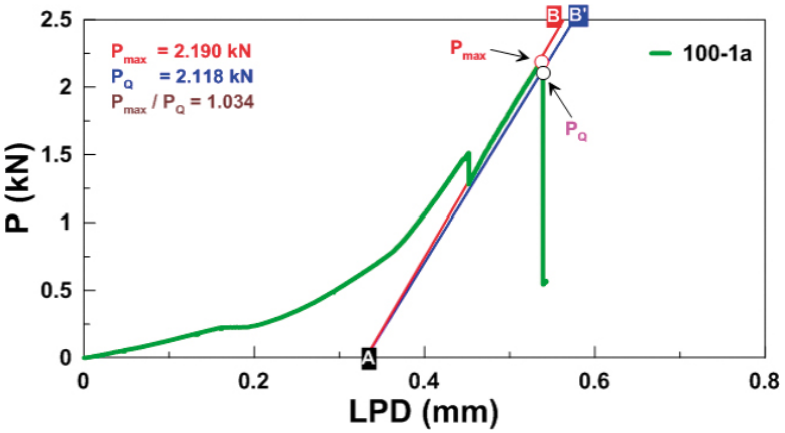

Figure A2- 2. *Experimental results of the SCB test performed with specimen 100-1a and verification of the linearity criterion of the compliance method. See text for explanation. Notes: P = applied horizontal load; P_{max} = maximum load; P_Q = conditional load; LPD = load point displacement.*

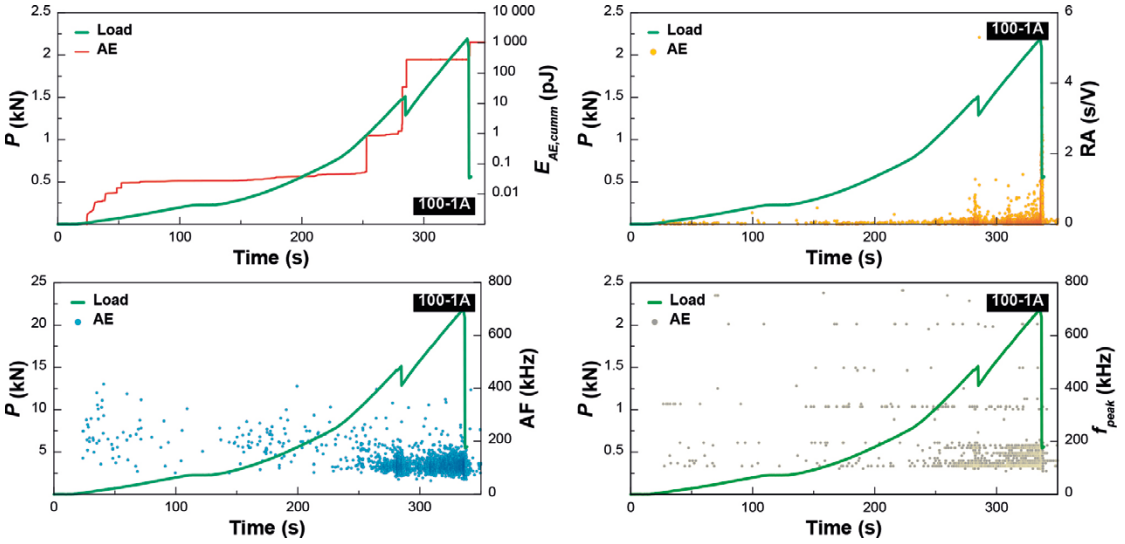

Figure A2-3. *Acoustic emission data associated with the SCB test performed with specimen 100-1a. Notes: P = applied horizontal load; $E_{AE,cumm}$ = cumulative acoustic energy; RA = rise angle (rise time/peak amplitude); AF = average frequency (counts/duration); f_{peak} = peak frequency.*

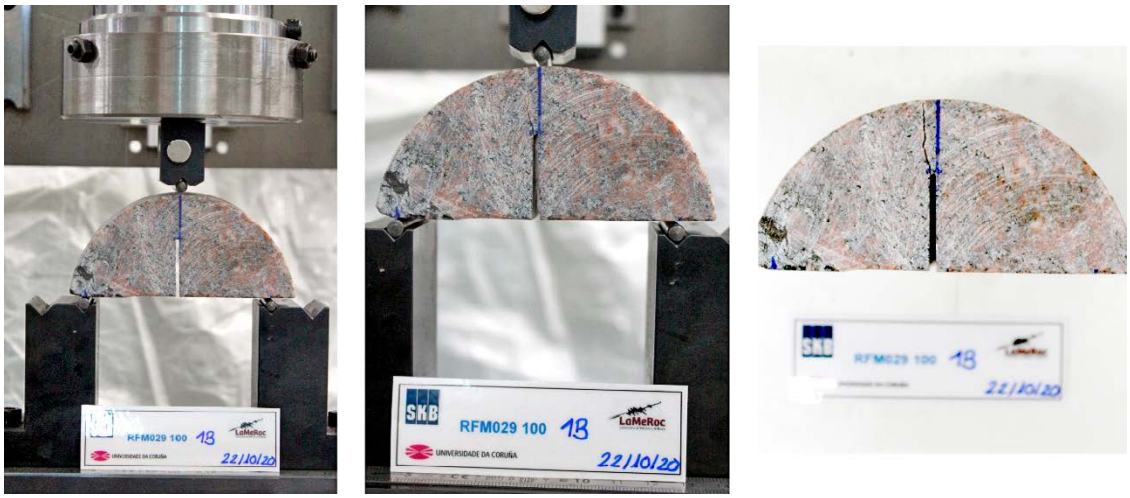

Figure A2-4. *Sample 101057 100-1b before (left) and after (middle and right) conducting a SCB test. The KIC value obtained was of 0.99 MPa m1/2 obtained for a maximum load of 2.24 kN.*

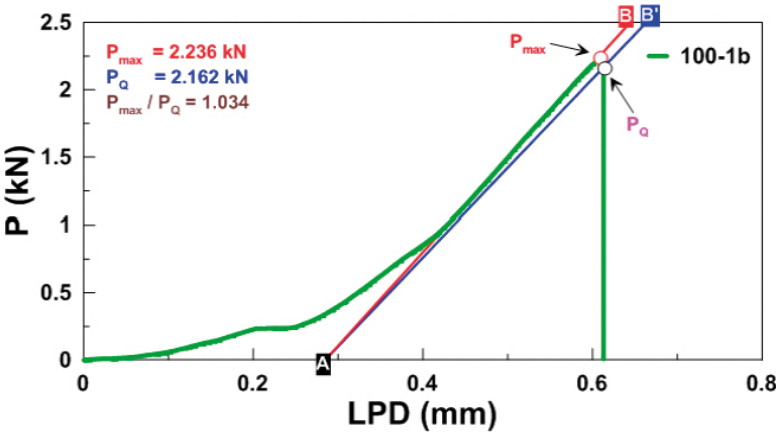

Figure A2-5. *Experimental results of the SCB test performed with specimen 100-1b and verification of the linearity criterion of the compliance method. See text for explanation Notes: P = applied horizontal load; P_{max} = maximum load; P_Q = conditional load; LPD = load point displacement.*

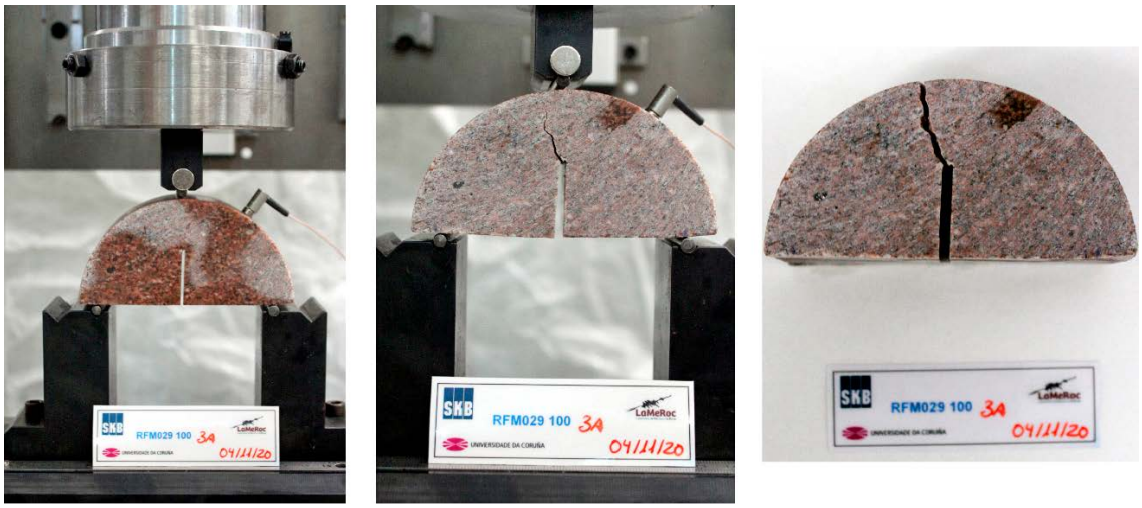

Figure A2-6. *Sample 101057 100-3a before (left) and after (middle and right) conducting a SCB test. The K_{IC} value obtained was of 1.76 MPa $m^{1/2}$ obtained for a maximum load of 4.04 kN.*

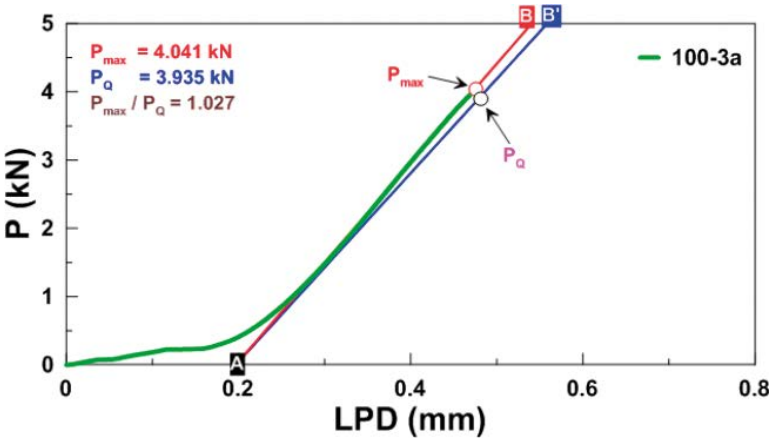

Figure A2-7. *Experimental results of the SCB test performed with specimen 100-3a and verification of the linearity criterion of the compliance method. See text for explanation Notes: P = applied horizontal load; P_{max} = maximum load; P_Q = conditional load; LPD = load point displacement.*

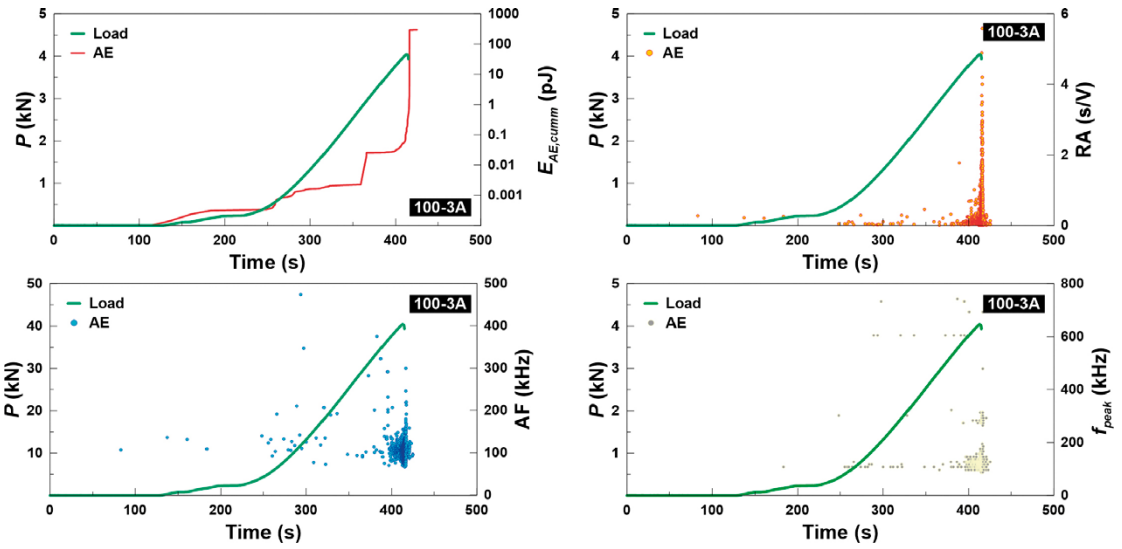

Figure A2-8. *Acoustic emission data associated with the SCB test performed with specimen 100-3a. Notes: P = applied horizontal load; $E_{AE,cumm}$ = cumulative acoustic energy; RA = rise angle (rise time/peak amplitude); AF = average frequency (counts/duration); f_{peak} = peak frequency.*

Figure A2-9. *Sample 101057 100-3b before (left) and after (middle and right) conducting a SCB test. The KIC value obtained was of 1.36 MPa m1/2 obtained for a maximum load of 3.13 kN.*

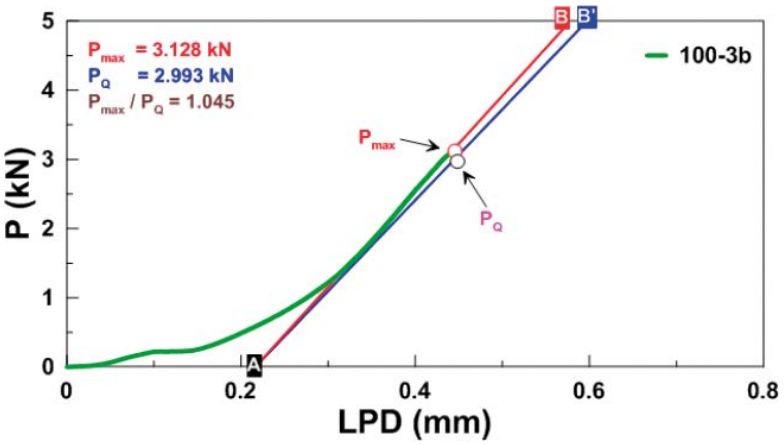

Figure A2-10. *Experimental results of the SCB test performed with specimen 100-3b and verification of the linearity criterion of the compliance method. See text for explanation Notes: P = applied horizontal load; P_{max} = maximum load; P_Q = conditional load; LPD = load point.*

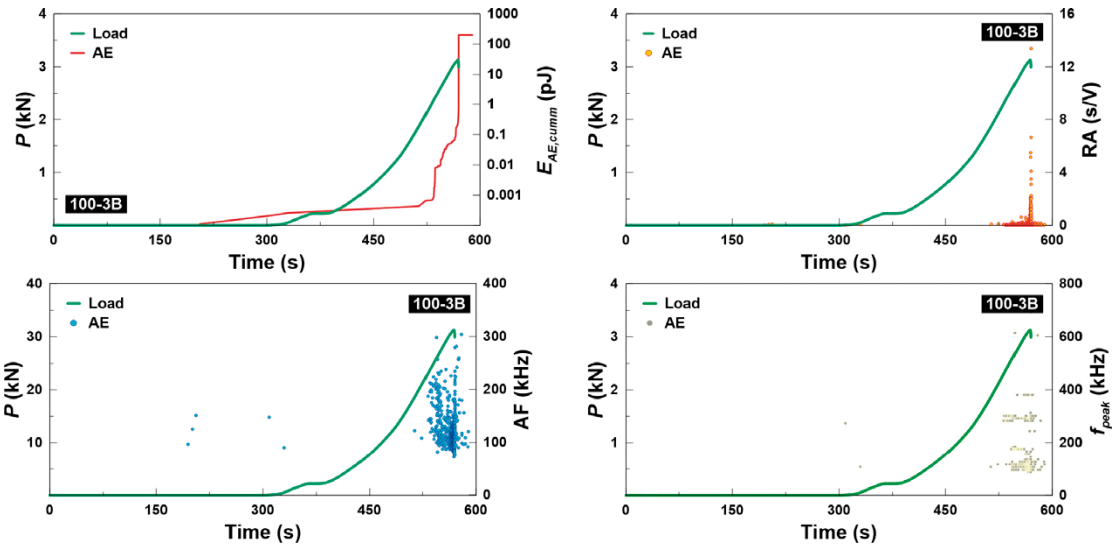

Figure A2-11. *Acoustic emission data associated with the SCB test performed with specimen 100-3b. Notes: P = applied horizontal load; $E_{AE,cumm}$ = cumulative acoustic energy; RA = rise angle (rise time/peak amplitude); AF = average frequency (counts/duration); f_{peak} = peak frequency.*

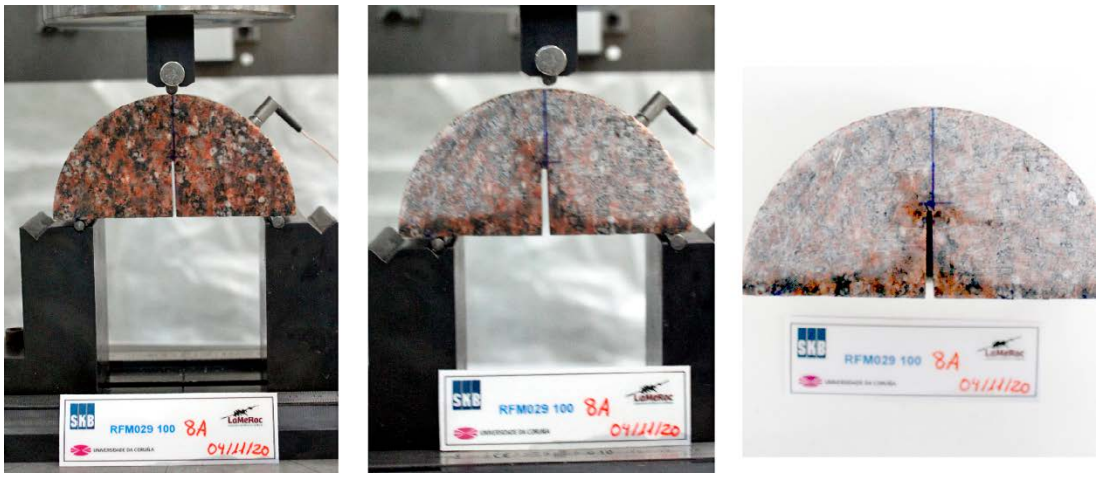

Figure A2-12. *Sample RFM029 100-8a before (left) and after (middle and right) conducting a SCB test. The K_{IC} value obtained was of 1.99 MPa $m^{1/2}$ obtained for a maximum load of 4.07 kN.*

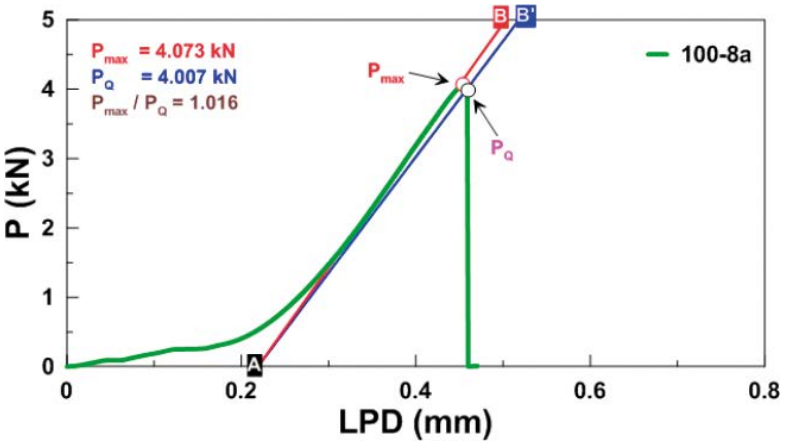

Figure A2-13. *Experimental results of the SCB test performed with specimen 100-8a and verification of the linearity criterion of the compliance method. See text for explanation Notes: P = applied horizontal load; P_{max} = maximum load; P_Q = conditional load; LPD = load point displacement.*

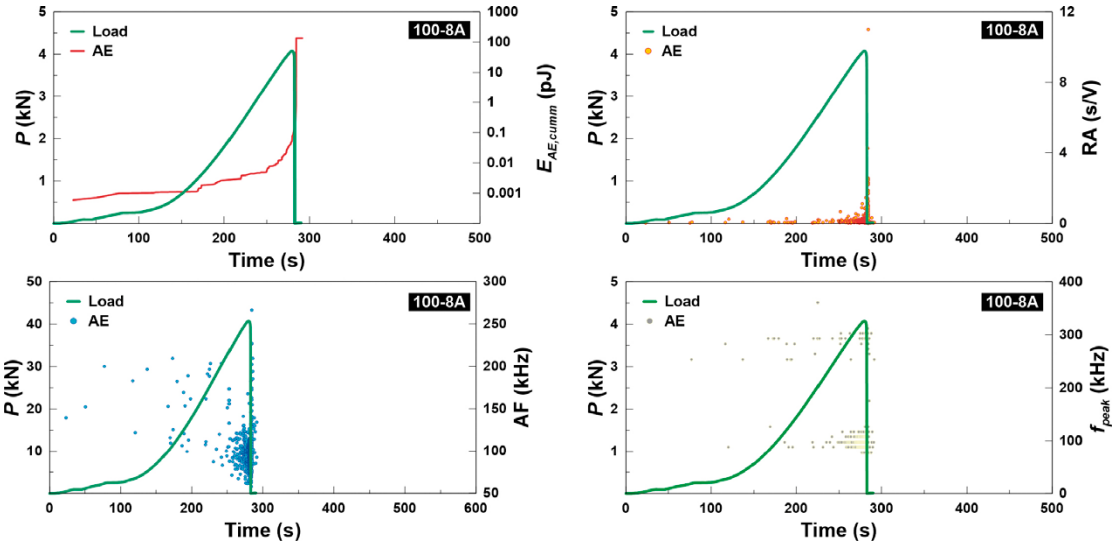

Figure A2-14. *Acoustic emission data associated with the SCB test performed with specimen 100-8a. Notes: P = applied horizontal load; $E_{AE,cumm}$ = cumulative acoustic energy; RA = rise angle (rise time/peak amplitude); AF = average frequency (counts/duration); f_{peak} = peak frequency.*

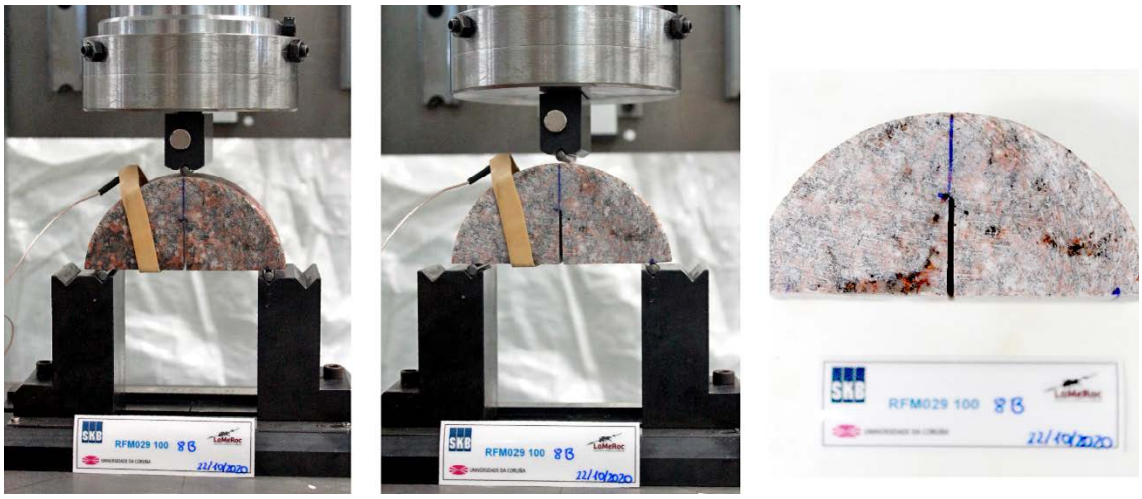

Figure A2-15. *Sample 101057 100-8b before (left) and after (middle and right) conducting a SCB test. The K_{IC} value obtained was of 1.15 MPa $m^{1/2}$ obtained for a maximum load of 2.36 kN.*

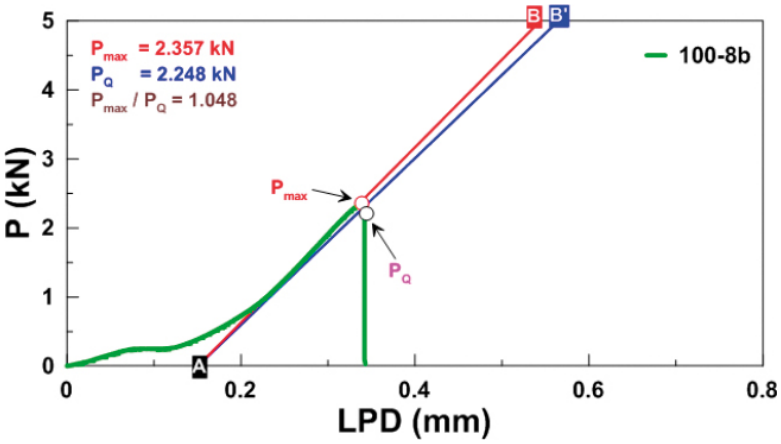

Figure A2-16. *Experimental results of the SCB test performed with specimen 100-8b and verification of the linearity criterion of the compliance method. See text for explanation Notes: P = applied horizontal load; P_{max} = maximum load; P_Q = conditional load; LPD = load point displacement.*

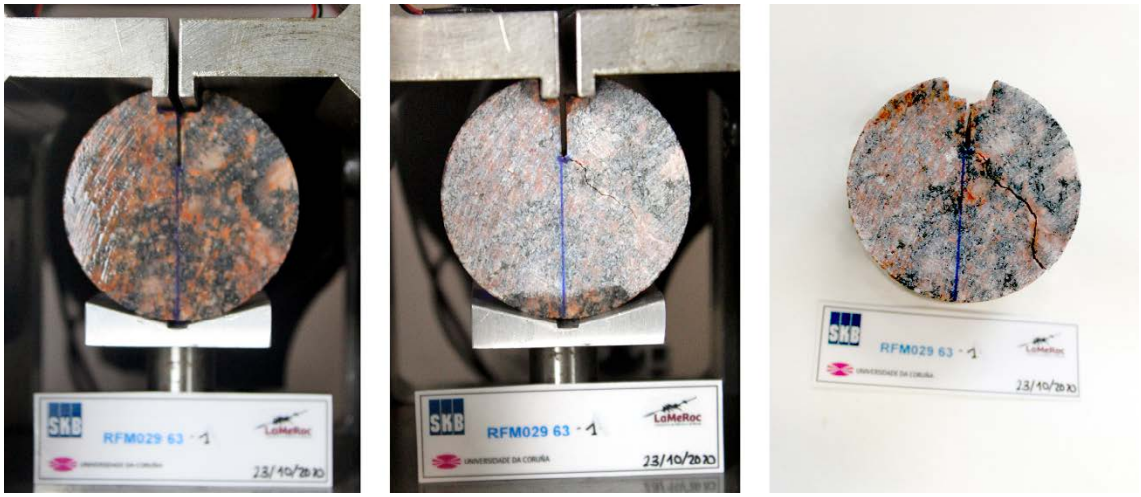

Figure A2-17. *Sample 101057 63-1 before (left) and after (middle and right) conducting a pCT test. The K_{IC} value obtained was of 1.38 MPa $m^{1/2}$ obtained for a maximum load of 1.49 kN.*

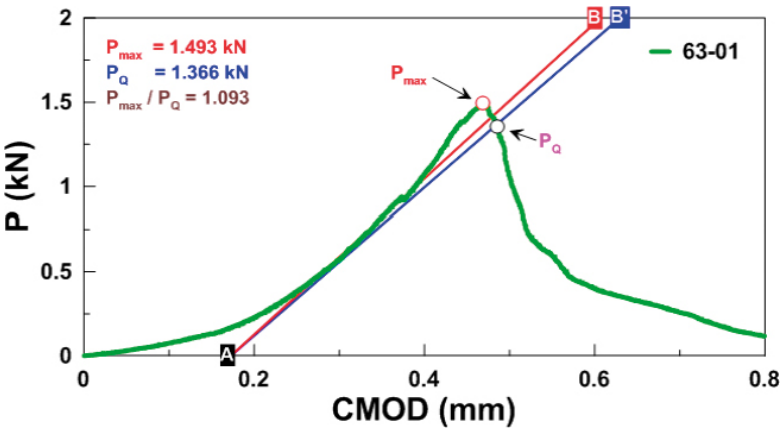

Figure A2-18. *Experimental results of the pCT test performed with specimen 63-01 and verification of the linearity criterion of the compliance method. See text for explanation Notes: P = applied horizontal load; P_{max} = maximum load; P_Q = conditional load; CMOD = crack mouth opening displacement (≡ load point displacement).*

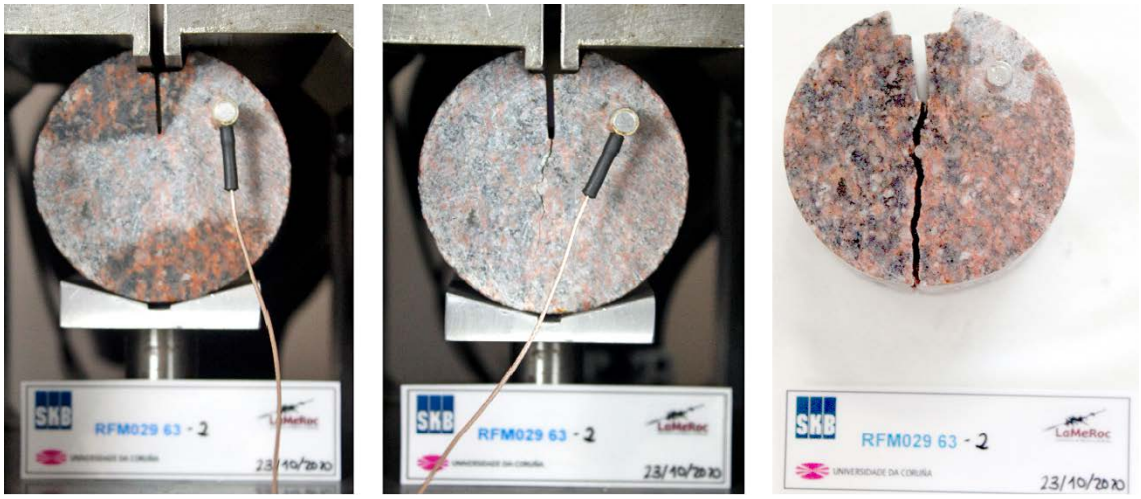

Figure A2-19. *Sample 101057 63-2 before (left) and after (middle and right) conducting a pCT test. The K_{IC} value obtained was of 1.87 MPa $m^{1/2}$ obtained for a maximum load of 2.04 kN.*

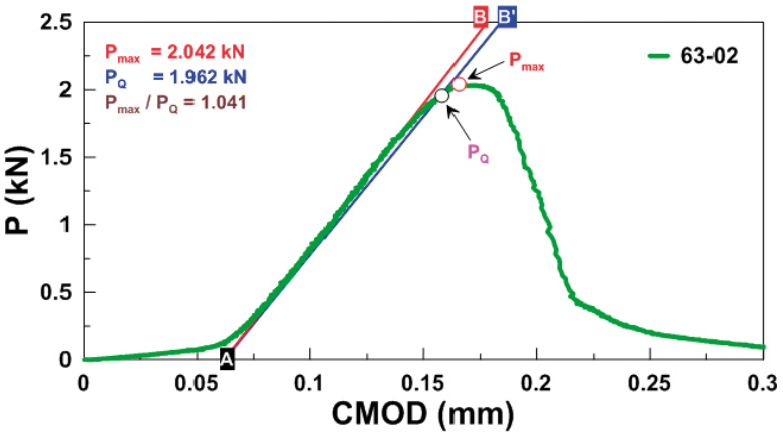

Figure A2-20. *Experimental results of the pCT test performed with specimen 63-02 and verification of the linearity criterion of the compliance method. See text for explanation Notes: P = applied horizontal load; P_{max} = maximum load; P_Q = conditional load; CMOD = crack mouth opening displacement (≡ load point displacement).*

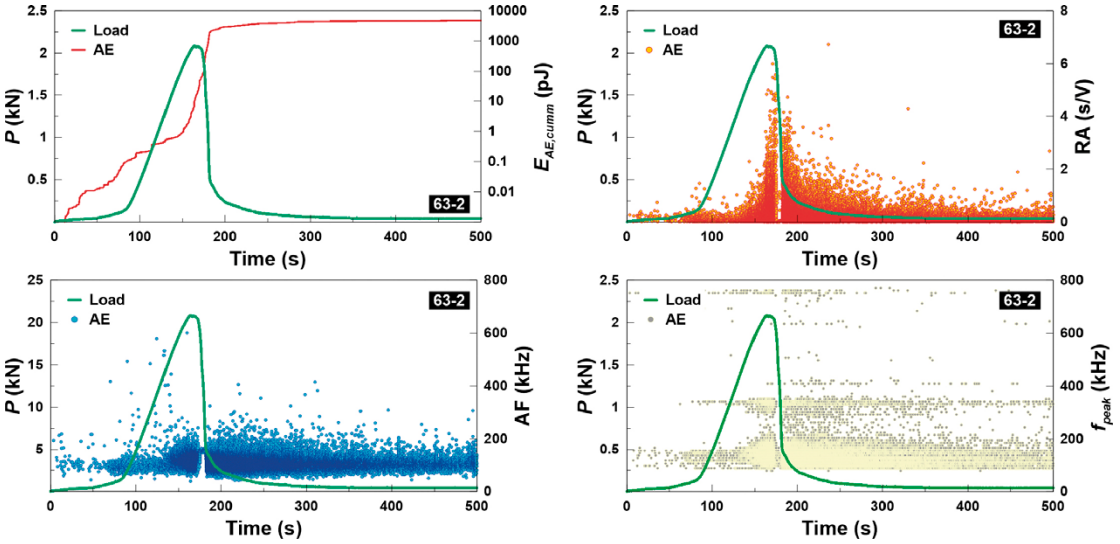

Figure A2-21. *Acoustic emission data associated with the pCT test performed with specimen 63-2. Notes: P = applied horizontal load; $E_{AE,cumm}$ = cummulative acoustic energy; RA = rise angle (rise time/peak amplitude); AF = average frequency (counts/duration); f_{peak} = peak frequency.*

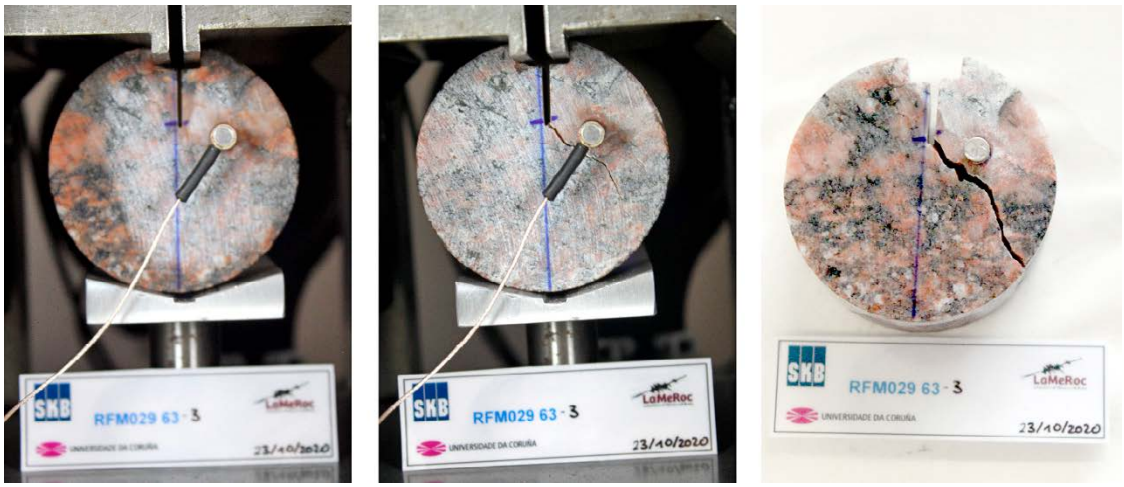

Figure A2-22. *Sample 101057 63-3 before (left) and after (middle and right) conducting a pCT test. The K_{IC} value obtained was of 1.61 MPa $m^{1/2}$ obtained for a maximum load of 1.78 kN.*

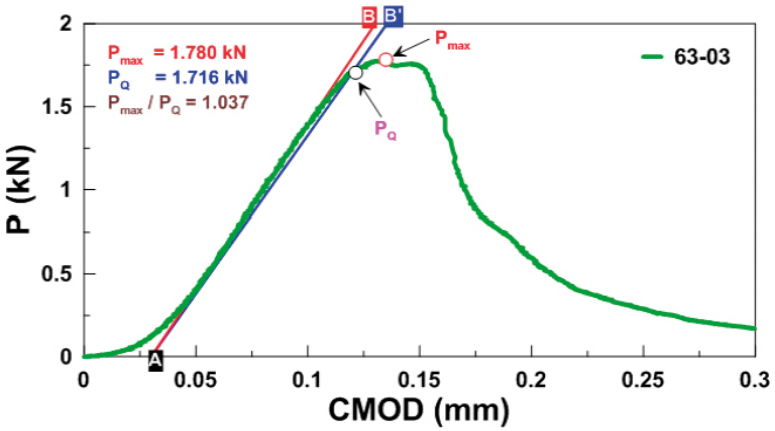

Figure A2-23. *Experimental results of the pCT test performed with specimen 63-03 and verification of the linearity criterion of the compliance method. See text for explanation Notes: P = applied horizontal load; P_{max} = maximum load; P_Q = conditional load; CMOD = crack mouth opening displacement (≡ load point displacement).*

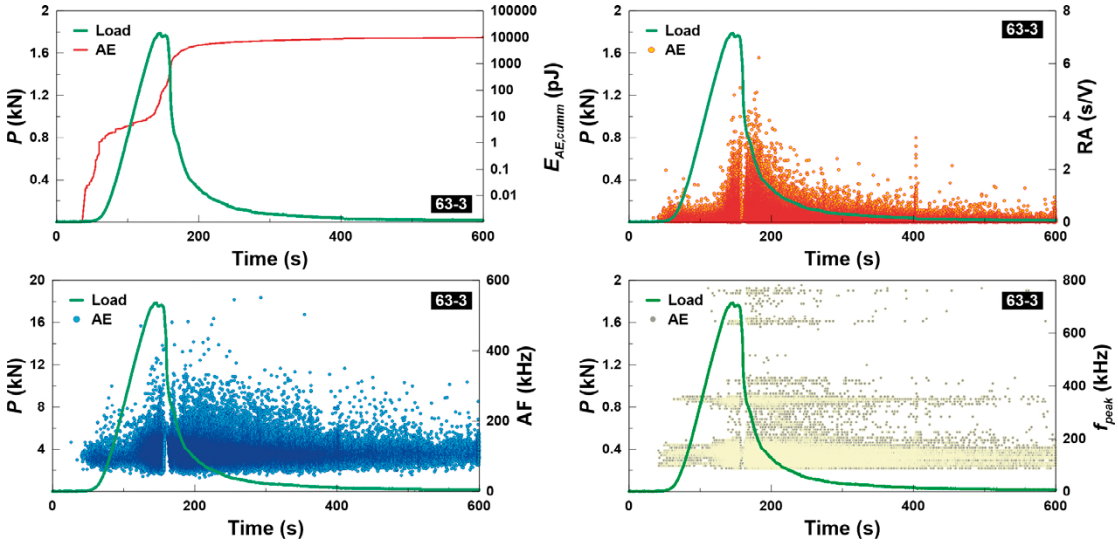

Figure A2-24. *Acoustic emission data associated with the pCT test performed with specimen 63-3. Notes: P = applied horizontal load; $E_{AE,cumm}$ = cumulative acoustic energy; RA = rise angle (rise time/peak amplitude); AF = average frequency (counts/duration); f_{peak} = peak frequency.*

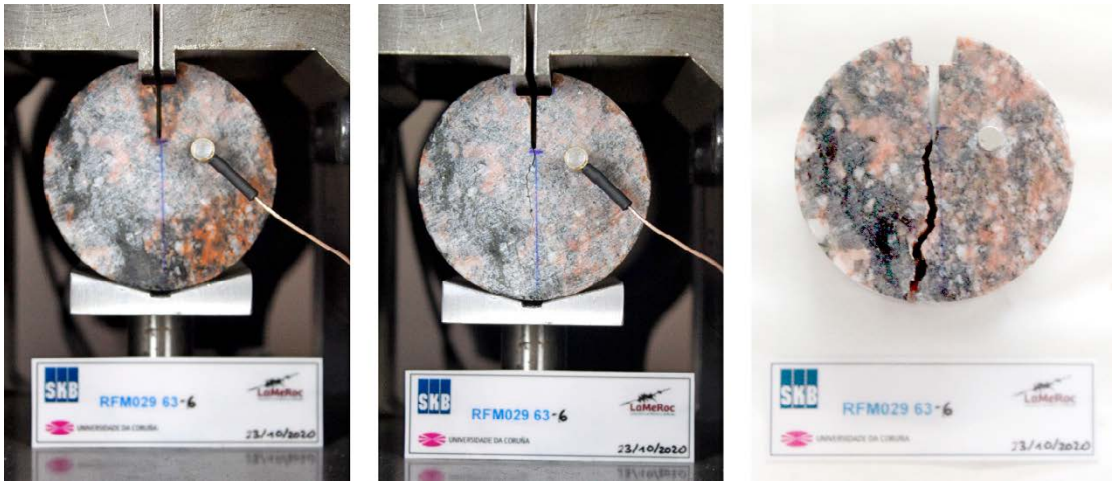

Figure A2-25. *Sample 101057 63-6 before (left) and after (middle and right) conducting a pCT test. The K_{IC} value obtained was of 1.52 MPa $m^{1/2}$ obtained for a maximum load of 1.71 kN.*

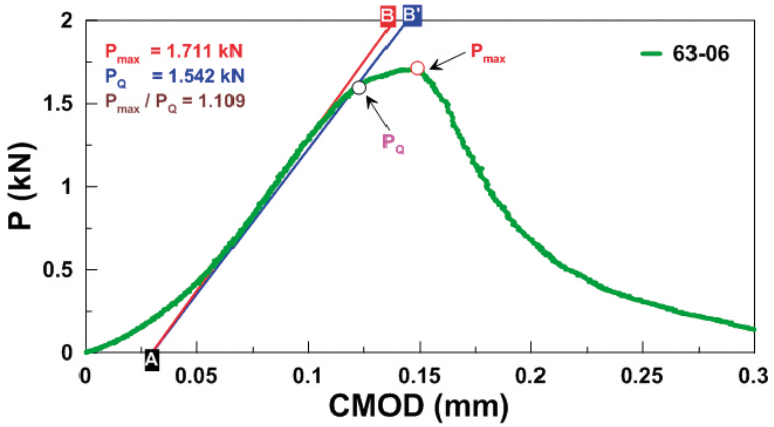

Figure A2-26. *Experimental results of the pCT test performed with specimen 63-06 and verification of the linearity criterion of the compliance method. See text for explanation Notes: P = applied horizontal load; P_{max} = maximum load; P_Q = conditional load; CMOD = crack mouth opening displacement (≡ load point displacement).*

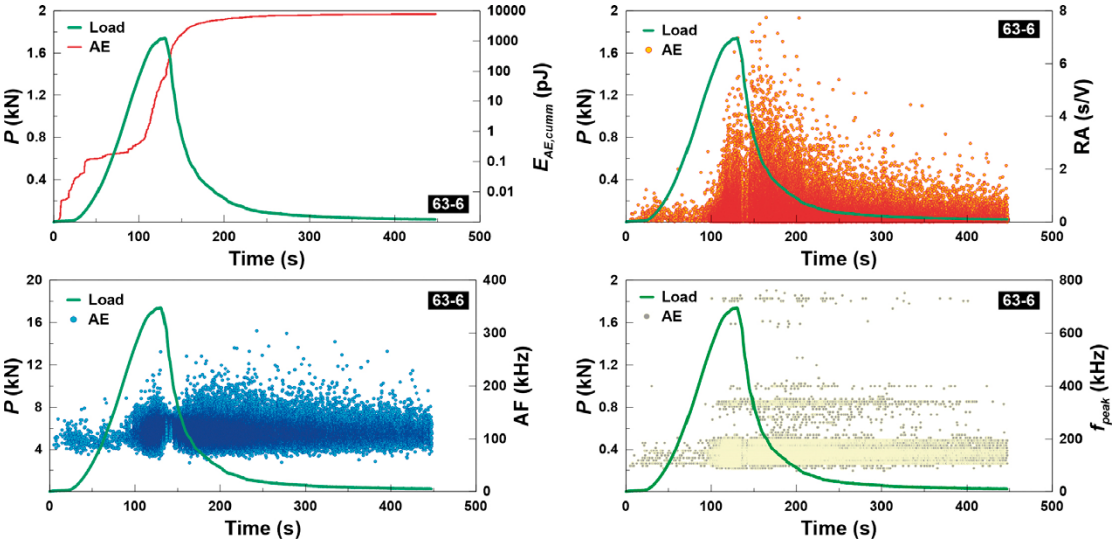

Figure A2-27. *Acoustic emission data associated with the pCT test performed with specimen 63-6. Notes: P = applied horizontal load; $E_{AE,cumm}$ = cumulative acoustic energy; RA = rise angle (rise time/peak amplitude); AF = average frequency (counts/duration); f_{peak} = peak frequency.*

Figure A2-28. *Sample 101057 63-11 before (left) and after (middle and right) conducting a pCT test. The K_{IC} value obtained was of 1.84 MPa $m^{1/2}$ obtained for a maximum load of 1.94 kN.*

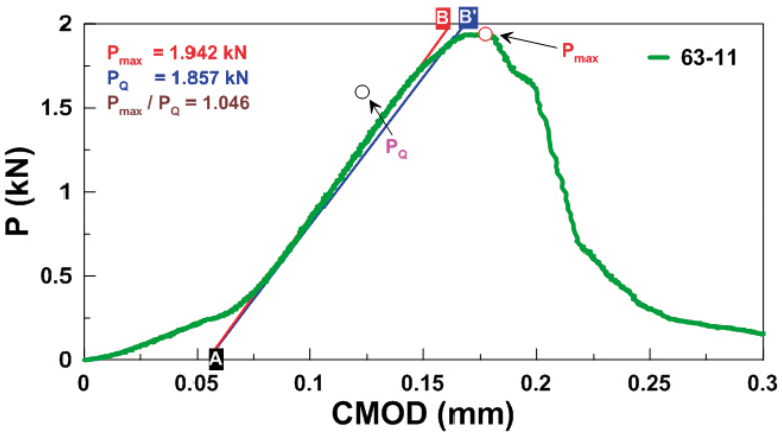

Figure A2-29. *Experimental results of the pCT test performed with specimen 63-011 and verification of the linearity criterion of the compliance method. See text for explanation Notes: P = applied horizontal load; P_{max} = maximum load; P_Q = conditional load; CMOD = crack mouth opening displacement (≡ load point displacement).*

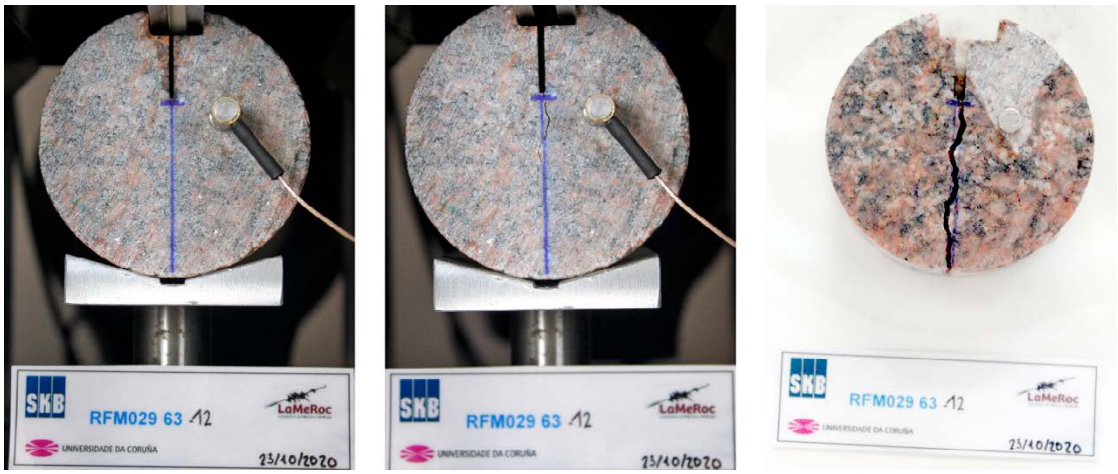

Figure A2-30. *Sample RFM029 63-12 before (left) and after (middle and right) conducting a pCT test. The K_{IC} value obtained was of 1.63 MPa $m^{1/2}$ obtained for a maximum load of 1.67 kN.*

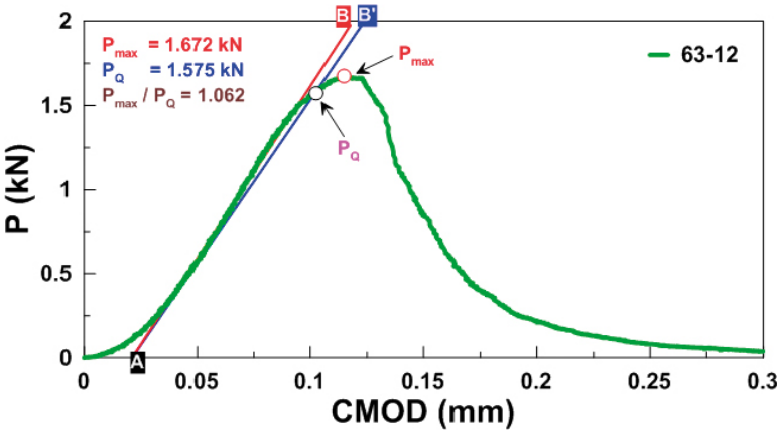

Figure A2-31. *Experimental results of the pCT test performed with specimen 63-12 and verification of the linearity criterion of the compliance method. See text for explanation Notes: P = applied horizontal load; P_{max} = maximum load; P_Q = conditional load; CMOD = crack mouth opening displacement (≡ load point displacement)*

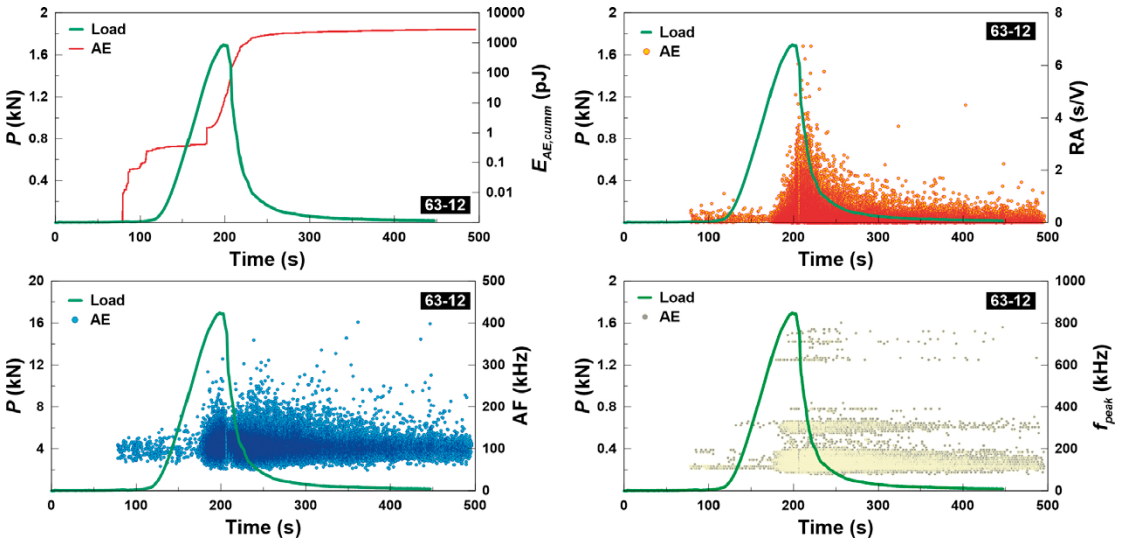

Figure A2-32. *Acoustic emission data associated with the pCT test performed with specimen 63-12. Notes: P = applied horizontal load; $E_{AE,cumm}$ = cumulative acoustic energy; RA = rise angle (rise time/peak amplitude); AF = average frequency (counts/duration); f_{peak} = peak frequency*

Arkitektkopia AB, Bromma, 2021

SKB is responsible for managing spent nuclear fuel and radioactive waste produced by the Swedish nuclear power plants such that man and the environment are protected in the near and distant future.

skb.se